Mälardalen University Press Licentiate Theses
No 72

CFD Modelling and Experimental Studies of the Fluid Flow and Heat Transfer in Copper Heat Sink Design

Bijan Karimpourian
2007

Department of Public Technology
Mälardalen University

ISBN 978-91-85485-44-4
ISSN 1651-9256
Printed by Arkitektkopia, Västerås, Sweden
Distribution: Mälardalen University Press

Utveckling av koppar kylare till datorer

Om vi förställer oss kunskapen som ett träd, växer vissa grenar av detta träd snabbt och andra långsamt. En oharmonisk tillväxt verkar föreligga hos kunskapsträdet. Hinder för tillväxten undersöks och reds ut kontinuerligt. Människan kan inte vänta på få uppfinnare och uppfinningar. Idag rensas hinder bort istället med hjälp av moderna hjälpmedel.
Industrier och varor är representanter för historiens progressionsgrad. Modellering av industriprocesser är ett verktyg som stöder elimineringen av godsutvecklingshinder.
Datorer är modellerings- och simuleringsfullbordande plattformen som accelererar evolutionen i samhället. Idag kräver näringslivet en snabbare utveckling av datorer som ska beskriva komplexa processer i industrier. Konstruktionen av snabba och starka datorer har blivit en akut fråga för samhället. Datorer kan inte klara av simulering av industrins komplicerade mål när till och med små komponenter är mycket komplexa. Varje liten bit ska läsas av datorn vid simulering av industrielement.
Processorer kan inte klara av att läsa miljarder bits av förloppsdetaljer. Att kräva större uppgifter av processorer medför utveckling av energi i form av värme i dem. Temperaturen hos varje komponent har en stor roll i dess prestationsförmåga. Det finns en omvänd relation mellan temperatur och kapaciteten av komponenter. Om temperaturen i utrustningen ökar så försämras dess prestation. Omvänt, så avlägsnas värmen från utrustningar förbättras deras förmåga. Målet med projektet har varit att avlägsna värmen från processorer genom utvecklingen av datorkylare.
Det är obestridligt att koppar är bästa material för värmeöverföring p.g.a. dess höga termiskförmåga. Men nuvarande datorkylare tillverkas av aluminium, som har en lägre värmeledningsförmåga (k).
Denna forskning omfattar materialundersökning, värmeöverföring och ny designer av kylare.
Materialegenskapsundersökningen i projektet består av att välja bästa tjocklek for flänsar av kylaren. Utformning av kylaren är förknippad med materialegenskaper, ekonomiska, industriella och termiska aspekter.
Densitet, volym, böjningsförmågan av utvalda flänsar, kostnader, värme kapacitans, värmeöverföringstal, tryckfall och fläktplacering är några av de variabler som ska beaktas. Effekten av värmeledning jämfört med konvektion ska undersökas. Förkastliga egenskaper hos kopparmaterialet med avseende på tillverkningsprocessen ska kompenseras med ny flänskonfiguration. Flänsprofil förslås som en lösning för termisk styrning, utöver ytlig area och större flödeshastighet.
Den nya kylaren ska modelleras och simuleras med CFD (Computational Fluid Dynamic).
Mekanisk konstruktion av kylaren ska studeras. Brazingteknik är också ett alternativ inför kopparkylaretillverkning. Tillverkning av kylaren av så kallade Louveredflänsar ska undersökas ur designaspekter. Experimentella försök ska bidra till att avgöra prestationen av Louveredflänskylaren.
Experimentellt arbete ska utföras med känsliga apparater för mätning av värme kapacitet av nya utformningar. En tredimensionell modell av kylaren utförs inom Gambit och modeller simuleras med Fluent. Prototyper optimeras inom CFD-miljö för att minimera manuellt arbete.

Abstract

In this thesis the heatsinks are analyzed and new designs for copper sinks are developed. Modeling and simulation by CFD, construction of prototypes and experimental work has been involved in this investigation. Challenges and complications in manufacturing of copper sinks are expressed and introduction to solutions of these hindrances is implicated in this work. Numerical effort has been made by fluent to promote investigation and in order to approach the goal, in which serves the new opportunities for wider application of copper material in heat sinks.

However the thermal conductivity of copper is about double as aluminum but still aluminum heatsinks are commonly used for heat dissipation in computers.
Comparing of heat performance of two analogous cooling devices of different materials, aluminum and copper, is conducted by numerical analysis in the CFD environment.
In addition to larger surface area and airflow velocity another solution for enhancement of heat dissipation is suggested.

Manufacturing solutions of copper heat-ejectors are proposed which will facilitate fabrication of more high performance copper heatsinks than the current heavy and expensive models.

Our first copper heat sink model is designed exclusively based on the technical considerations and analyses of numerical simulation of two identical copper and aluminum heat-ejectors by CFD and as well as manufacturability concerns.

The proposed heatsink is fabricated mechanically and is tested by a number of heat sources and high sensitive devices such as adhesive K type thermocouple, data acquisition 34970A in associated with HP Bench Link program.

An extent experimental work on aluminum cooling devices, integrated with forced convection, is performed in order to measure the thermal capacities.

Comparison of the heat performance of a typical aluminum cooling device, which was the best among the all aluminum cases and the proposed copper model under identical experimental conditions, is performed.

Also in some numerical efforts, optimizing and predicting of the thermal characterization of the copper approach with inclined free fins is developed. The model is scaled up in the fluent environment to predict its application in the cooling of larger heat generated electronic devices.
Impingement air-cooling mode of force-convection is adopted for heat dissipation from high power electronic devices in associated with the proposed inclined fin model.

Components of airflow velocity in the hollow spaces of the extended surfaces are discussed. Pressure drop and other thermal variables are analyzed analytical and by CFD code.

Another mechanical manufactured copper heat sink is investigated. A new design of the base and fins is optimized.
Three-dimensional finite volume method is developed to determine the thermal performance of the offered cooling device.

Thermal and hydraulic characterization of the heat sink under air-forced convection cooling condition is studied. The flow behavior around the fins and some other parts of the heat sink is analyzed by utilizing CFD code.

The hydraulic parameters including velocity profiles, distribution of static pressure, dynamic pressure, boundary layer and fluid temperature between the fins and in the passageway at the middle of the heat sink are analyzed and presented schematically.

Furthermore the thermal characteristic of the copper approach of cooling is studied by utilizing the contours of the three dimensional temperature distributions through the fins and temperature of the heat source by CFD code.

List of appended papers and review

This thesis is based on the following papers and review:

Paper1. Bijan Karimpourian & Jafar Mahmoudi, Some important considerations in heatsink design, presented at Eurosime 2005, 18-20 April, Berlin, Germany,

Paper2: Bijan Karimpourian & Jafar Mahmoudi, Experimental determination of the thermal performance of a free standing fin structure copper heatsink, Accepted at Sims 2005, 13-14 October, Norway

Paper 3: Bijan Karimpourian, Jafar Mahmoudi, Mark Irwin, Numerical and experimental study of the inclined free fins applied for thermal management submitted to the journal of numerical methods of heat and mass transfer:Emerald

Paper 4: Bijan Karimpourian, Jafar Mahmoudi, and Mark Irwin, 3-Dimensional numerical and analytical study of flow and thermal behavior of proposed mechanical fabrication of copper heat sink, submitted to Journal of Green energy

Backup material:

Bijan Karimpourian, Jafar Mahmoudi "A review to Electronic Cooling devices", 2005, ISBN 91-88834-73-5
(This review consists of 70 pages and only the abstract is included in this thesis.)
Registered at Mälardalen University

Acknowledgement

I have to be sincerely thankful from:

1. *My supervisor, Jafar Mahmoudi PhD at Outokumpu & adjunct professor at MdH*
2. *Richard Nipple PhD at R & D Outokumpu in Vasteras*
3. *Mark Irwin PhD at Outokumpu fabrication technology*
4. *Professor Erik Dahlquist at Mälardalen University*
5. *Adel Karim, PhD and researcher at Mälardalen university*
6. *Lars Wester, professor and prefect at Mälardalen University*
7. *Stig Andesson at workshop of Outokumpu R& D*
8. *Gert Bard at laboratory of Mälardalen University*
9. *Bengt Arnryd lecturer i VVS technology at Mälardalen university*
10. *Robert Ömen senior lecturer at Mälardalen university*
11. *Outokumpu research and development division in Vasteras for their partial supporting*
12. *Technical support of Fluent in Gothenburg*

Nomenclature

A	Area [m^2]
A_f	Each individual channel frontal area, [m^2]
A_{fc}	Through channel cross sectional area of the heatsink, [m^2]
A_o	Frontal area of the heatsink [m^2]
A_s	Total surface area of the heatsink in contact with the flow, [m^2]
A_{tf}	Entire heatsink frontal area, [m^2]
b	Base thickness, [m]
C_p	Specific heat at constant pressure [j/kg K]
d	Pin diameter, pin (fin) hydraulic diameter, [m]
D	Fin density, fin area density
D_h	Hydraulic diameter of the channel, [m]
f	friction factor
$f\,app$	Hydrodynamic developing flow apparent friction
g	gap, Width of the heatsink gap [mm]
h	height, [m], heat transfer coefficient [w/m^2k]
H_f	Height of the fin [m]
k	loss factor, thermal conductivity
K	Boltzmann constant (equation 1), thermal conductivity [W/m k]
K_c	Contraction loss coefficient
K_e	Expansion loss coefficient, loss factor
l	Length
L	Total length of the fin
n	Number of pins or fins
m	Mass
N	Number of fins
p	Fin pitch
P_e	Thermal performance
q"	Heat flux [W/m^2]
Q	Rate of heat dissipation W, flow rate [m^3/s]
$\dot{Q}_b$	Flow rate through the heatsink [m^3/s]
$\dot{Q}_0$	Flow rate for a heatsink with zero tip and lateral clearances [m^3/s]
R	Thermal resistance [°C/W]
Ra	Average roughness [1/(length)]
Re	Reynolds number
R_q	Root-mean-square roughness 1/[length]
R_{cs}	Thermal resistance between the junction and case
R_{ja}	Thermal resistance between the junction and ambient
R_{jc}	Thermal resistance between the junction and case
R_{sa}	Sink-ambient thermal resistance,
S_n	Surface normal unit vector
S_ϕ	Amount of ϕ generated in control Volume
S_k, S_ε	User defined source terms
S_h	Heat of chemical reaction
t	Thickness of a fin
t_f	Fin thickness, [m]

T	Temperature
T_a	Ambient air temperature in [°C]
T_c	Case temperature of the device
T_{cs}	Temperature difference between case and sink
T_{jc}	Temperature difference between junction and case
T_j	Maximum junction temperature of the device
T_s	Sink temperature
T_{sa}	Temperature difference between Sink and ambient
u	Flow velocity [m/s]
U	Overall heat transfer coefficient [w/m^2 K]
V	Velocity [m/s]
V_{ap}	Heat sink approach velocity, [m/s]
V_{ch}	Heat sink channel velocity, [m/s]
$\overline{V}_f$	Average flow velocity through the heatsink [m/s]
V_o	Velocity of the approach flow upstream of the heatsink [m/s]
W	Width of the heatsink
x, y, z	Rectangular coordinate [m]
x+	Hydrodynamic entrance length
Δp	Pressure drop, [pa]
ΔT	Temperature difference [^oC]
$\overline{\tau}_w$	Average shear stress in channels of heatsink
Pr	Prandtl number
$\overline{\Delta P}_o$	Overall pressure drop across the heatsink
$\overline{\Delta P}_f$	Frictional pressure drop
α	Geometric fraction
β	
ν	Kinematic viscosity, [m^2/s]
ρ	Density, [kg/m^3]
∇	Three-dimensional Del operator
λ	Geometric fraction
μ	Dynamic viscosity [kg/s.m]
ϕ	Scalar quantity, two-dimensional spreading function
ψ_{max}	A function of thermal conductivity of heat sink, dimensionless spreading resistance

Table of contents

1. Introduction

From the microscopic point of view Kinetic energy originates from the motion of atoms and molecules. Kinetic energy is invisible on the atomic and molecular scale.
Molecules and atoms can posse three different motions and the microscopic kinetic energy is defined associated to these motions.

- *Translational*
- *Vibrational*
- *Rotational*

Microscopic potential energy
This energy is due to the intermolecular attraction forces and relative locations of two atoms in a molecule with respect to one another. More sophisticated potential energy function considers Steric and electrostatic interactions.

Internal energy
Internal energy involves the kinetic and potential energies, in the microscopic scale. Internal energy is separated from the apparent macroscopic energy of moving objects.

Temperature
Temperature is a measure of the average translational kinetic energy associated with the disordered motion of atoms and molecules.
Temperature measures only the kinetic energy part of internal energy and not whole the internal energy.

$$\left[\frac{1}{2}mV^2\right]_{Average} = \frac{3}{2}KT \tag{1}$$

If the amount of translational kinetic energy of two objects is equal they have also the same temperature but their internal energy and specific heat will not necessarily be the same.
Two objects are in thermodynamic equilibrium when they have the same temperature. Any external velocity does not increase the internal energy, but the kinetic energy of whole system. Static temperature is calculated by the amount of the average kinetic energy of molecules.

Heat
Heat is energy in transfer resulting from difference in temperature through the medium and it travels in waves. Heat can be released through a chemical reaction or trapped by insulators. Heat originates from the motion of atoms and molecules in the matter. When thermal energy transfers from an object with higher temperature to another with lower temperature the molecules of the colder object vibrate faster and consequently the energy of the molecules enhances.

Heat transfer (or heat)
Heat is transferred in three ways, conduction, convection, radiation. Heat transfer by phase change including boiling and condensation are classified as the forms of the convection mode of heat transfer because they involve fluid motion.

Kinetic energy of molecules may be related to random translational motion, internal rotation and vibration motions.

Conduction

Conduction may be explained as the transfer of energy from particles at higher energy level to lower due to collision between them. Heat transfer by conduction in the materials occurs in different ways regarding to states and phases of materials. Conduction in the gases and liquids is associated to diffusion of energy due to molecular activity. Molecular interactions in liquids are stronger and more frequent than gases. When energy is transferred within a solid that is not fluent, heat transfer is of conduction mode. Conduction in a solid conductor is the transfer of motions including atoms in the form of lattice vibrations and translational motion of free valence electrons. In the nonconductors energy transfer is due to lattice waves that are induced by atomic motions.

Convection

If the flow of heat is transferred from a solid surface to the boundary layer of a fluid by conduction, the kinetic energy of molecules of the fluid at the interface increases, and the distance between molecules is extended associated to more interactions induced by more energetic molecules. The density of hot regions decreases due to expansion and the cold surrounding is denser. Hot fluid rises (macroscopic movement) due to buoyancy force and energy is transferred by molecules with higher energy from less dens regions to dens regions through the fluid. Convection is heat transfer through the fluids (i.e. liquids and gases) this means that heat moves with fluid.

Conductive heat transfer is directly proportional to cross section area and convective heat transfer equation is proportional to surface area of fins or bodies subjected to the airflow

Conductive heat transfer equation (Fourier's law)

For one dimensional plane wall with a temperature distribution across the medium the rate of heat transfer in Cartesian coordinates is proportional to the product of temperature gradient and cross section area of the wall.

$$Q = -KA\frac{dT}{dx} \qquad \text{1-Dimensional} \tag{2}$$

In the case of the dimensional temperature gradient through a wall with a constant cross section area and thermal conductivity the rate of heat flux through the wall is proportional to temperature gradient.

$$q'' = -K\nabla T \qquad \text{3-Dimensional} \tag{3}$$

Convective heat transfer equation: (Newton's law of cooling)

The heat transfer rate is related to the overall temperature difference between the wall and fluid and the surface area.

$$Q = h\, A_s\, (T_s - T_a) \tag{4}$$

The quantity h is called the convection heat transfer coefficient

Thermal conductivity

Thermal conductivity is an intensive property of materials that expresses the magnitude of energy rate (energy per second) that can transfers through a matter with 1 m^2 cross section (heat flux, q") when the temperature difference is 1 k per meter (temperature gradient dT/dx).

Thermal conductivity or heat transfer coefficient shows the ability of the materials to conduct heat and is expressed in W/m K. The rate of heat transfer (q) depends upon the temperature gradient and the thermal conductivity of the material.
Thermal conductivity = heat flow rate × thickness / (cross section area × temperature difference)
The measure of how good a material is at conducting heat is known as its thermal conductivity. Metals have a high thermal conductivity, due to the availability of freely movable valence electrons, while non-metals (with their electrons bound to the nuclei), normally have low thermal conductivity. Thermal conductivity of copper is about double as aluminum. (K_{Al}= 237 W/m k, K_{Cu}= 401W/m k).

2. Heatsinks: Enhancement of heat transfer

Temperature of a component has a great role in determining the performance of the equipment. This effect is a conclusion of an inversely relationship between the component's temperature and its thermal performance. As the temperature of the implement increases consequently its performance decreases. Removing the heat from hot surfaces of implements is a matter of study in which has many industrial applications.
To enhance the heat dissipation rate from any hot surface, the extension of the heated surface by adding the fins is a thermal solution. Plate fins and pin fins are two modes of extended surfaces.

The cooling device is attached to the hot surface of any apparatuses in order to increase the surface area and therefore reduces the temperature of the devices by improving the heat dissipation from the hot zones. One of the major applications of the extended surfaces is cooling the CPUs of computers.
Development of the computers by decreasing the size of components and a simultaneous increasing the heat generation of these components, intensify the necessity of advanced heat-ejectors.

Heat dissipation from the computers can accomplish by using the extended surfaces, cold fluids or a combination of these two solutions.
Traditional desktop computer design relied on natural convection from a heatsink placed directly on the processor. But with elevation of the power of processors, new computers relay on force convection i.e. a fan is added to these heat sinks. Improvement of heat-removals continues as long as technology is developing.

2. A review to Heatsinks and theoretical concepts

At present time the current cooling technologies are developing in the following areas.

- Synjets
- Pin fin heatsink
- Plate fin heatsink
- Heat pipes
- Micro channels
- Vapor Chamber

This study discuss exclusively fabrication and development of copper plate heat-ejectors but before we proceed and focus on the experimental and numerical investigation it is noteworthy to discuss cooling devices including common terms and equations applied for evaluation of current plate sinks.

2.1 Thermal resistance (R) and thermal circuit

Thermal resistance indicates the temperature difference between two points per unit of heat rate dissipation between them and is related to thermal conductivity of the materials across the two points and some other factors depending on type of thermal resistance.

$$R = \Delta T/Q \tag{5}$$

The unit of thermal resistance is in °C/W. To have an idea about this resistance we consider a heatsink attached to a heat generated apparatus as shown in the figure1.

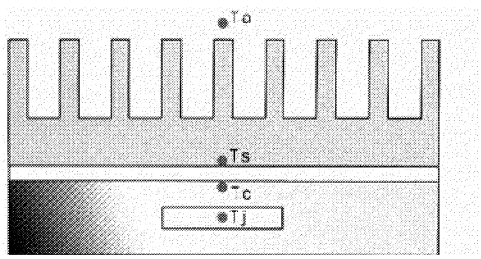

Figure1: Major thermal resistances at sectors of a cooling process [1]

Heat is generated at the junction and then dissipated by conduction as heat transfers across the junction to case and further to the extended surfaces and finally removed by convection to environment.

Thermal circuit represents the heat flow via different materials schematically it is analogous to electrical thermal resistance. Circuit representation is a useful tool for both conceptualizing and quantifying heat transfer problems and it can give an understanding of total heat dissipation process as well. Thermal circuit resistance of this system is drawn in the next figure.

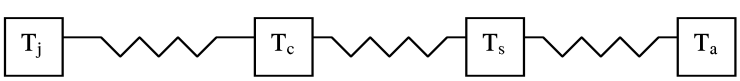

R_{jc} R_{cs} R_{sa}

Figure 2: Thermal circuit resistance representing the involved resistances in above heatsink

The thermal partial resistance at any zone of the circuit may be computed by equation (5) when ΔT is difference temperature between two locations.
When two locations are respectively junction and case then the thermal resistance between these two parts is expressed as following:

$$R_{jc} = (T_{jc})/Q = (T_j - T_c)/Q \quad (6)$$

Where
T_{jc} indicates the difference temperature between junction and case of source of heat.

Case- sink thermal resistance (interface resistance):

R_{cs} represents the thermal resistance between the base of heat-ejector and the case of the source and this resistance may be accounted by next equation.

$$R_{cs} = (T_{cs})/Q = (T_c - T_s)/Q \quad (7)$$

This resistance arises from the existence of an interface between two zones. If this value is too high it is possible to modify it either by using alternative interface material or improve the contact surfaces. The conductivity of the interface material is relevant in heat dissipation from the heat sources when using the heatsink.
Improvement of the contact surface is affected also by factors such as flatness, thickness of applied pressure and size of the contact area.

Sink-ambient thermal resistance:
This resistance is calculated by the next equation theoretically.

$$R_{sa} = (T_{sa})/Q = (T_s - T_a)/Q \quad (8)$$

T_{sa} indicates the temperature difference between the ambient and the sink.

Heatsink thermal resistance

$$R_{sa} = ((T_j - T_a)/Q) - R_{jc} - R_{cs} \quad (9)$$

This relation can be applied for selection the required cooling device. Since the air temperature participates in this equation and Q is convection heat transfer therefore, h (heat transfer coefficient) is involved as well. Heat transfer coefficient is a function of other factors such as dimension and orientation of the heat removing tools, and air flow modes (i.e. natural, forced, and mixed).

Total junction-to-ambient resistance

$$R_{ja} = R_{jc} + R_{cs} + R_{sa} = (T_j - T_a)/Q \quad (10)$$

2.2 Heatsink selection

The selection of a cooling device rely on the largeness of the heat traffic i.e. input and output heat through the implement. The output heat depends on external condition of the cooling instrument such as airflow modes (i.e. natural, forced, mixed) and the geometry. The input heat depends on the power and the heat flux of the heatsource.

2.3 Localization and shape of the heat source

Shape of the heat source determines the shape of the base hence they must match each other. Since they have not the same contact area thus the localization of the heat source at the base affect the thermal spreading resistance and hence the heat performance will be changed.
The spreading resistance is greater when a heat source is located at the edge or corner of a heat sink.

2.4 Thermal spreading resistance

When the heat spreads from the heat source across the heatsink, a problem takes place with regarding to the fact that both have different contact area. Normally, heat sources have smaller cross section area than the base of the cooling tools. Development of the heat from a small area to a larger region causes a resistance due to different cross section area.

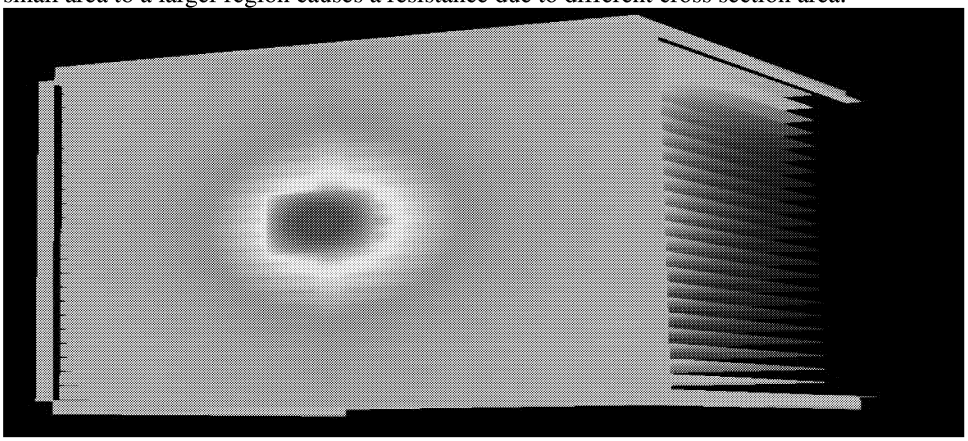

Figure 3: The hot spot produced at the bottom and horizontal heat spreading across a typical sink is displayed

The higher thermal spreading resistance, the larger hot spot develops on the device. It is not easy to diminish this effect regarding to design considerations.
Thermal spreading resistance is shown in the figure 3. Hot spot is produced at the center of the sink. This subject is elaborated in subsequent sections including the theoretical calculations and numerical presentation.

2.5 Fan & jet blowing approaches (SISE & TISE)

There are two modes of "fan location" and "jet blowing direction". The first approach is traditional mode called SISE (side-inlet, side-exit), which means that the fan is placed beside the instrument and blows through it and the exiting air flows out of the heatsink from the opposite side. Another configuration is TISE (top-inlet, side-exit) in which a jet or axial fan is mounted directly above the implement and it blows the air down into the spaces of fin arrays. TISE is perpendicular to the base of the device but SISE is mounted parallel to the base.
TISE flow provides a 20% performance enhancement. [12]
TISE flow is a solution to avoid stagnating flow in the traditional fan placement.

2.6 Impingement flow

Impingement flow is generated by collision of fluid onto the surface. The liquids or gases are injected or sprayed onto the surface and strike the surface with high velocity. Around the impact region, the boundary layer is very thin because the fluid hits the surface with a high

force, which makes the boundary layer very thin, and therefore heat transfer is easier. Impingement flow is associated with the TISE mode of fan location.
Figure (4) shows the impingement flow configuration and defines the geometries of the structure. The channel height is H, the inlet width W, channel spacing s, channel length L, impingement velocity U.

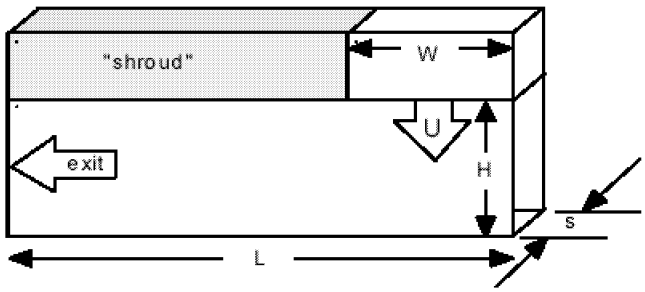

Figure4: Representation of a type of impingement flow [7]

2.7 Fin tip clearance

Clearance ratio is defined as ratio of the distance between the top of the exiting jets (airflow) over the fins and fin tips to the fin height (h/H in figure 5). Fin tip clearance can vary from zero, which means there is no flow bypass, to a finite value. This phenomenon takes place in concerned with impingement flows.
Pressure loss coefficient resulting from TISE jet-impingement decreases as the tip clearance increases.
Higher tip clearances may result in lower heat transfer rate. Zero tip clearance gives much higher heat transfer coefficient than tip clearances with higher value. [5]

2.8 Parallel Plate fins

The generated heat in the electronic components bodies must be removed by conduction as well as convection. Heat is lost initially by conduction through the surfaces or walls of the heat-generated body but furthermore it must be dissipated by convection to the surrounding.
Extended surfaces refer commonly to a solid that transfer the heat by conduction within its boundaries and then by convection between its boundaries and the surroundings. Extended surfaces enhance the heat transfer rate between the hot body and ambient by convection. Such extended surfaces are the fins of cooling instrument.
Different fin configurations are suggested. The basic types of fins are plate fins and pin fins.
The convection heat transfer at the corresponding surface (that is extended by the fins) of the heat generated surface result in the difference temperature between the two opposite wall of the body and provides the temperature gradient inside the body.

2.9 Parallel plate correlations

By using the computational fluid dynamic it is possible to approximate some variables to determine heat transfer rate and other quantities necessary to characterize the flow through the heatsink. Correlations applied for CFD depends on facility to approximate the variables. For example determining the fin velocity based on the upstream flow rate in the enclosure is often difficult. We must consider the phenomenons concerning the heat-ejectors and their relations on hydraulic parameters of these devices.

2.10 Flow bypass

Flow bypass can be determined by the ratio of flow rate through the heatsink to the flow rate for a sink with zero tip and lateral clearances. [5]

$$\frac{\dot{Q}_b}{\dot{Q}_o} = 1 - \frac{\overline{V}_f A_{fc}}{V_o A_o} \tag{11}$$

Both $\overline{V}_f$ (average flow velocity through the heatsink) and V_o (velocity of the approach flow upstream of the heatsink) may be obtained from the applied CFD (an element base control volume). $\dot{Q}_b$ is the exiting volumetric flow rate over the instrument representing the flow bypass and $\dot{Q}_o$ is the volume flow rate incident on upstream face of implement. A_{fc} is the through-channel cross sectional area of the cooling tool and Ao is the frontal area of that.

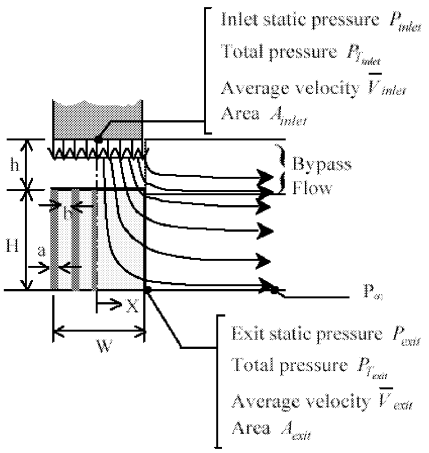

Figur5: Flow bypass through a typical heatsink [13]

2.11 Total pressure drop across the heatsink ΔP_o

The total pressure drop across the cooling device arises from the shear stress between the fluid and the solid surface and losses due to expansion or contractions, which the former is directly associated with the geometry.

2.12 Frictional and Loss factor

Friction factor is a dimensionless frictional pressure drop and a correlation for this factor is introduced in the literature. [5]

$$f = \frac{\overline{\tau}_w}{1/2 \rho V_o^2} \tag{12}$$

Where the $\overline{\tau}_w$ is the average shear stress in the channels of the heatsink, which may be calculated directly by CFD. The fluid properties such as viscosity are directly proportional to the friction factor.

Loss factor that is an acceleration component of the pressure drop results from sudden change of the flow area at the instrument. This quantity is accounted in associated to the geometry of the heatsink. Loss factor is calculated in some literatures using the following correlation. [5]

$$k = \frac{\Delta p}{\left(\frac{1}{2}\rho U^2\right)} \tag{13}$$

Where ΔP is pressure drop and U is the average inlet flow speed.
Contraction loss coefficient and expansion loss coefficient are related to the geometry of the cooling device but apparent friction factor is related to both geometry and channel velocity.

Airflow entering the heat-ejector is affected by contraction and the airflow pressure falls and the contraction loss coefficient may be computed in this concern. When the airflow exits the cooling device then it is affected by expansion. When the flow is in transition from the developing flow to fully develop flow, the dimensionless pressure drop is called the apparent friction. Apparent friction is a hydrodynamic loss. Contraction and expansion loss coefficient are affected by exclusively the geometry of the heatsink but calculating the apparent friction factor involves both geometry and channel velocity V_{ch}.

2.13 Channel velocity

The air accelerates when it passes through the channels of the heat-ejector. Approach velocity is a scale with a scaled factor to estimate the channel velocity. The scale factor is typically the ratio of the plate geometry, width of the gaps, b, and the fin thickness, t_f. [6]

$$V_{ch} = V_{ap}\left(1 + \frac{t_f}{b}\right) \tag{14}$$

But the modified channel velocity with more accuracy employs a new scale factor with the ratio between the sum of each individual channel frontal area A_f and entire heatsink frontal area A_{tf}.

$$V_{ch} = V_{ap}\left(1 + \frac{A_f}{A_{tf}}\right) \tag{15}$$

In the following these two channels velocities accuracy will be examined.
H = height, g = gap, t = fin thickness, b = base thickness, L = fin length, W = width (length)of the sink

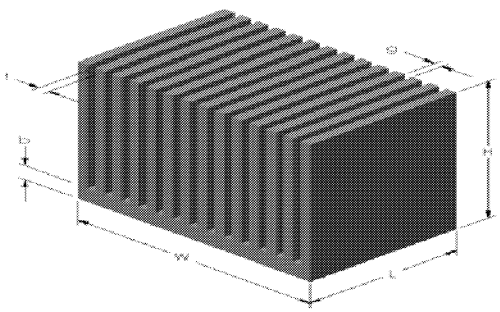

Figure 6: Demonstration of a heat sink with its geometry [6]

By estimating the channel velocity the total pressure drop can be computed.

2.14 Empirical equations for pressure drop calculations

Three theoretical pressure drop equations for parallel flows through the heatsinks are suggested. Correlations are compared with experiments and numerical calculations. These equations [6] are expressed as

1-

$$\Delta P = \left(\frac{f_{app} N(2HL + bL)}{HW} + K_c + K_e \right) \left(\frac{1}{2} \rho V_{ch}^{\ 2} \right) \tag{16}$$

2-

$$\Delta P = \left(4 f_{app} x^+ + K_c + K_e \right) \left(\frac{1}{2} \rho V_{ch}^{\ 2} \right) \tag{17}$$

3-

$$\Delta P = 4 \left(f_{app} x^+ + K_c + K_e \right) \left(\frac{1}{2} \rho V_{ch}^{\ 2} \right) \tag{18}$$

The variables applied in these equations are discussed below.

2.15 Hydrodynamic developing flow apparent friction, f_{app}

The hydrodynamic developing flow apparent friction f_{app} is related to hydrodynamic entrance length, x+, and the fully developed laminar flow friction factor.

$$f_{app} \operatorname{Re}_{ch} = \left[\left(\frac{3.44}{\sqrt{x^+}} \right)^2 + \left(f \operatorname{Re}_{ch} \right)^2 \right]^{1/2} \tag{19}$$

Where

$$x^+ = \frac{L}{D_h \operatorname{Re}_{ch}} \tag{20}$$

2.16 Channel Reynolds Number

Channel Reynolds Number, Re_{ch} is given by

$$\operatorname{Re}_{ch} = \frac{V_{ch} D_h}{\nu} \tag{21}$$

2.17 The fully developed laminar flow friction factor

The fully developed laminar flow friction factor, *f,* can be computed from the following:

$$f \operatorname{Re}_{ch} = 24 - 32.53\beta + 46.72\beta^2 - 40.83\beta^3 + 22.96\beta^4 - 6.09\beta^5 \tag{22}$$

Where

$$\beta = \frac{b}{H} \tag{23}$$

2.18 The contraction and expansion loss coefficients

The following expressions are contraction loss coefficient, K_c and expansion loss coefficient, K_e, for airflow entering and exiting the heat sinks with rectangular channels:

For equation (18)

$$K_c = 0.42(1-\alpha^2) \tag{24}$$

$$K_e = (1-\alpha^2)^2 \tag{25}$$

For equation (19)

$$K_c = 0.8 - 0.4\lambda^2 \tag{26}$$

$$K_e = (1-\lambda^2) - 0.4\lambda^2 \tag{27}$$

For equation (20)

$$K_c = 0.8 + 0.04\beta - 0.44\beta^2 \tag{28}$$

$$K_e = (1-\beta)^2 - 0.4\beta^2 \tag{29}$$

Where

$$\alpha = 1 - \frac{Nt_f}{W} \quad , \beta = \frac{b}{H} \ , \ \lambda = \frac{b}{b+t_f} \tag{30),(31),(32}$$

2.19 Friction factor and Nusselt number (Gneilinsky formula)

Relationship between dimensionless form of pressure drop and Nusselt number is presented by a more accurate formula suggested by Gneilinsky.

$$Nu_D = \frac{(f/2)(\mathrm{Re}_D - 10^3)\,\mathrm{Pr}}{1+12.7(f/2)^{1/2}(\mathrm{Pr}^{2/3}-1)} \tag{33}$$

2.20 Some other applicable equations:

Prandtl number:

$$pr = \frac{\mu c_p}{k} \tag{34}$$

Reynolds number

$$\mathrm{Re} = \frac{\rho u D_h}{\mu} = \frac{u D_h}{\nu} \tag{35}$$

- *Fin efficiency*

$$\eta_f = \frac{\tanh(m.H_f)}{m.H_f} \tag{36}$$

Where H_f is the fin height or fin length depending on whether fin is in horizontal or vertical condition and m is defined as below:

$$m = \sqrt{\frac{2.h}{k_{fin}.t_{fin}}} \tag{37}$$

3. Computation method

An extensive part of our work including optimization, simulation, design, predicting of flow behavior and heat transfer is carried out by CFD code. That is why it is relevant to introduce an introduction to CFD.
CFD is an abbreviation for Computational Fluid Dynamics that is the analyzing and predicting of systems involving flow, heat transfer and associated phenomena such as chemical reactions by means of computer- based simulation.
By using CFD, a computational model that represents a system or device is built. This model can be studied later.
CFD enable us to design a device or a system that is difficult to prototype or test experimentally and see how it performs.
It is possible to test many variations until you reach the optimal result.
The effectiveness of an implement may be investigated under a given set of circumstances.
A CFD simulation consists of three stages. The first step is pre-processing including construction of 2D or 3D of the model, creating and applying a suitable computational mesh, and entering the flow boundary conditions and fluid materials properties. Building the model can be performed by CAD or by GAMBIT.
The next step is adopting the governing equations of the model and solving them in the new environment that is fluent.
The CFD solver does the flow calculations and produces the results.
CFD solvers are usually based on the finite volume method. CFD applies numerical methods (called Discretization) to develop approximations of the governing equations of fluid mechanics and the fluid region to be studied.
The flow region or calculation domain is divided (discretize) into a large number of finite volumes or cells. This Discretization is straightforward for very simple geometries such as rectangles or circles, but is a difficult problem in CAD for more complicated objects.
General conservation (transport) equation for mass, momentum, energy, etc., are discretize into algebraic equations.
All equations are solved to render flow field. Fluid flows are modeled by a set of partial differential equations, the Navier--Stokes equations.
On the discretize mesh, the Navier-Stokes equations take the form of a large system of nonlinear equations; going from the continuum to the discrete set of equations is a problem that combines both physics and numerical analysis.
Systems of equations are solved simultaneously to provide solution.
Post processing is the third step and is the final step in CFD analysis involving the organization and interpretation of the predicted flow data and the production of CFD images and animations. High-resolution images and animations help you to tell your story in a quick and impactful manner such as domain geometry and grid displaying, vector plots, particle tracking and view manipulation (translation, rotation, scaling etc.). Reliability of CFD-based predictions is never 100% which can be related to the inaccuracy of input data, the power of available computer may be too small for high numerical accuracy and the scientific knowledge base may be inadequate. The reliability is greater in regard to following considerations:

- For laminar flows rather than turbulent ones
- For single-phase flows rather than multi-phase flows;
- For chemically-inert rather than chemically-reactive materials;
- For single chemical reactions rather than multiple ones;
- For simple fluids rather than those of complex composition.

4. Governing equations of numerical computation

- *General transport equation*

$$\frac{\partial}{\partial t}\int_{v}\rho\phi dV+\oint_{A}\rho\phi V.dA=\oint_{A}\Gamma\nabla\phi.dA+\oint_{V}S_{\phi}dV \tag{38}$$

Unsteady convection diffusion generation

This equation includes the unsteady state, convection, diffusion and generation terms of scalar parameterϕ.
Simulation is derived in the steady state condition and therefore this equation reduces to:

$$\oint_{A}\rho\phi V.dA=\oint_{A}\Gamma\nabla\phi.dA+\oint_{V}S_{\phi}dV \tag{39}$$

Diffusion term may be eliminated because the operation is conducted at single phase and

therefore general transport equation can be expressed as

$$\oint_{A}\phi\rho V.dA=\oint_{V}S_{\phi}dV \tag{40}$$

- *Energy equation*

The designs are modeled and optimized by CFD code which solves the energy equation in the

following form.

$$\frac{\partial}{\partial t}(\rho E)+\nabla.(\vec{\upsilon}(\rho E+p))=\nabla.\left(k_{eff}\nabla T-\sum_{j}h_{j}\vec{J}_{j}+(\overline{\overline{\tau}}_{eff}.\vec{\upsilon})\right)+S_{h} \tag{41}$$

The three terms in the parenthesis on the right hand side represent energy transfer due to conduction, species diffusion, and viscous dissipation. S_h includes the heat of chemical reaction. Energy is defined as below:

$$E=h-\frac{p}{\rho}+\frac{\upsilon^{2}}{2} \tag{42}$$

Each of the terms in this equation has the units of energy per mass.
Thermal dissipation is conducted under the conduction and convection operations and no chemical reaction is taken place so the last term in the right hand side of the energy equation is ignored. The fluid flows at low velocity and it has a low density so the effect of viscous dissipation may be insignificant and consequently we can ignore its effect. The thermal process is conducted at one phase condition and no mass transfer is occurred. Ultimately the process is performed under steady state condition. Therefore the energy equation also reduces to the following equation:

$$\nabla.(\vec{v}(\rho E + p)) = \nabla.\left(k_{eff} \nabla T\right) \tag{43}$$

Pressure work and kinetic energy terms are negligible in incompressible flows.

- *Continuity equation*

$$\frac{\partial \rho}{\partial t} + \frac{\partial \rho u}{\partial x} + \frac{\partial \rho v}{\partial y} + \frac{\partial \rho \omega}{\partial z} = 0 \tag{44}$$

This equation is valid for incompressible as well as compressible flows if there is no mass added to continuous phase in other words if flow including only one phase and no vaporization or phase change takes place. This equation also reduces to steady state condition form as below:

$$\frac{\partial \rho u}{\partial x} + \frac{\partial \rho v}{\partial y} + \frac{\partial \rho \omega}{\partial z} = 0 \tag{45}$$

If density is maintained constant the equation reduces further to:

$$\frac{\partial u}{\partial x} + \frac{\partial v}{\partial y} + \frac{\partial \omega}{\partial z} = 0 \tag{46}$$

- *Integral-volume momentum conservation equation*

$$\int_A (\rho u)(u.s_n)dA = -\frac{\partial}{\partial t}\int_V \rho u dV + \sum_i F_i \tag{47}$$

The first term on the left side of equation represent net rate of momentum flow out of the control surface (also called convective acceleration term).

The first and second terms on the right hand side of equation(47) illustrate respectively the rate of momentum storage in the control volume (local acceleration term) and the sum of all external forces acting on the control surface and volume; volumetric forces and surface forces: surface pressure, surface viscous stress tensor (N/m^2), volumetric gravitational force, ρg (N/m^3).

The above equation is applied for an inertial (non-accelerating) reference frame. Consequently with regard to the pointed circumstances the integral volume momentum conservation equation may simplify as below:

$$\int_A (\rho u)(u.s_n)dA = \sum_i F_i \tag{48}$$

- *Transport equations for the standard k-ε model*

Turbulent kinetic energy (k) and its rate of dissipation (ε) are obtained from the two following transport equations.

$$\frac{\partial}{\partial t}(\rho k) + \frac{\partial}{\partial x_i}(\rho k u_i) = \frac{\partial}{\partial x_j}\left[\left(\mu + \frac{\mu_t}{\sigma_k}\right)\frac{\partial k}{\partial x_j}\right] + G_k + G_b - \rho\varepsilon - Y_M + S_k \tag{49}$$

.

$$\frac{\partial}{\partial t}(\rho\varepsilon)+\frac{\partial}{\partial x_i}(\rho\varepsilon u_i)=\frac{\partial}{\partial x_j}\left[\left(\mu+\frac{\mu_t}{\sigma_\varepsilon}\right)\frac{\partial\varepsilon}{\partial x_j}\right]+ \\ C_1\varepsilon\frac{\varepsilon}{k}(G_k+C_{3\varepsilon}G_b)-C_{2\varepsilon}\rho\frac{\varepsilon^2}{k}+S\varepsilon \tag{50}$$

- *Turbulent viscosity for the standard k-ε*

The turbulent (eddy) viscosity, μ_t, is computed by combining k and ε as follows:

$$\mu_t=\rho C_\mu\frac{k^2}{\varepsilon} \tag{51}$$

5. Discretization

When the complexity of boundary conditions and geometries or nonlinearities does not allow solution of partial differential equations (PDE) by analytical methods, numerical methods are a solution and can be applied however these are the approximate solution of PDE.
Unlike the analytical solution that solves the equations for all points of the domain, the numerical methods support only discrete points and values are calculated at discrete places on a meshed geometry. Three essential Numerical techniques are introduced below however there are other methods.

1- Finite Element Method (FEM)
2- Finite Difference Method (FDM)
3- Finite Volume Method (FVM)

The objects are subdivided into smaller regions by numerical methods and approximate results are obtained for discrete points. Two approaches are used to discretize the PDEs.

1- Taylor series Discretization in FDM:
2- Control volume Discretization in FVM and FEM

Finite difference form of a function may be expressed by definition of derivative of the function. Taylor series expansion is used to develop the finite difference form of the derivative to obtain an algebraic equation of the function. These points are called nodal points or nodes. The aggregates of the nodes are termed the grid or mesh. Each node represents a certain region and any physical property of the node is the average property of the region.

In the control volume approach the computational domain is divided into non overlapping cells or small volumes and the partial differential equations applies to these volumes. Finite volume refers to the small volume surrounding each node point on a mesh. Usually these cells are polygons (triangles, quadrilaterals) in 2-D and polyhedral (tetrahedron, hexahedron, prisms, etc) in 3-D.

The variables are located at the centre of the control volume. The next step is to integrate the differential form of the governing equations over each control volume. Consider a single partial differential equation in conservation form

$$\frac{\partial u}{\partial t} + \nabla . f(u) = 0 \tag{52}$$

Where u is a conserved quantity and

$$f(u) = [f_1(u),..., f_d(u)] \text{ is the flux vector.} \tag{53}$$

Integrating this over any volume we get the integral form of the conservation law

$$\frac{\partial}{\partial t}\int_V u dx + \oint_{\partial V} f_i n_i ds = 0 \text{ and } (n_1,\ldots,n_d) \text{ is the unit outward normal to } \partial V \tag{54}$$

Conservation equations for each volume may be solved simultaneously. Volume integrals of partial differential equations are converted to surface integrals, using divergence theorem.

$$\int_V div(\rho u \phi) dV = \int_s \rho (u.n) \phi dS \qquad (55)$$

Because the flux entering a given volume is identical to that leaving the adjacent volume, these methods are conservative.

Surface integral is again split to a set of integrals over each of the faces bounding the control volume. The sets of algebraic equations determined from conversion of integral equations into discrete forms, using the mean value theorem, are obtained.

The system of algebraic equations can be expressed in the matrix form. There are two methods of solving matrix of algebraic equations, direct and iteration method.

Since these methods are approximate solutions, the accuracy can be examined by different techniques. Accuracy of FDM can be evaluated by the order of the truncation error in the Taylor series expansion and it is the difference between the exact solution of derivative and its finite difference expression.

But accuracy of FEM and FVM is more complicated because different Discretization schemes are available. FEM and FVM involve two types of errors, Round-off and truncation errors. When computation is not made in exact arithmetic the real numbers are represented in floating point form and errors are caused due to rounding-off the real numbers.

6. Material selection (Conduction effect)

Selection of the heatsink material is a crucial subject in manufacturing point of view because the type of applied materials has a major impact on cooling performance. Heat removing can be improved by using materials of higher thermal conductivity. Copper and Aluminum are two competitive candidates for heatsink material. (K_{Al}= 237 W/m k, K_{Cu}= 401W/m k). Copper has higher thermal conductivity and therefore the heat dissipation at conduction level should be accomplished far effective. This statement is corroborated by numerical efforts in the next capital.

A numerical study is performed to investigate the impact of the type of material used in manufacturing of the heat removing tools. Thermal performance of analogous heatsinks of different materials, aluminum and copper, is compared by CFD code. Geometry of the implements is remained constant but the applied materials change under simulation process. Varity of power and flow velocities are exerted to these instruments and the hydraulic behaviors are observed by numerical calculations of the physical parameters. Figure 7 and 8 are demonstrations of temperature distribution of two cooling devices.

The results turned out that the thermal performance of the copper case is much better than the aluminum type. The applied heat sources in this attempt represent the processors in computers or any other devices. Material selection of the sinks was the fundamental parameter that varied in the fluent under simulation when comparing the two cases. This implies that every simulation was performed twice one time for copper and next time for Aluminum. The base thickness was 2 mm and number of the fins was 48 with 0. 2 mm thickness.

Al heatsink

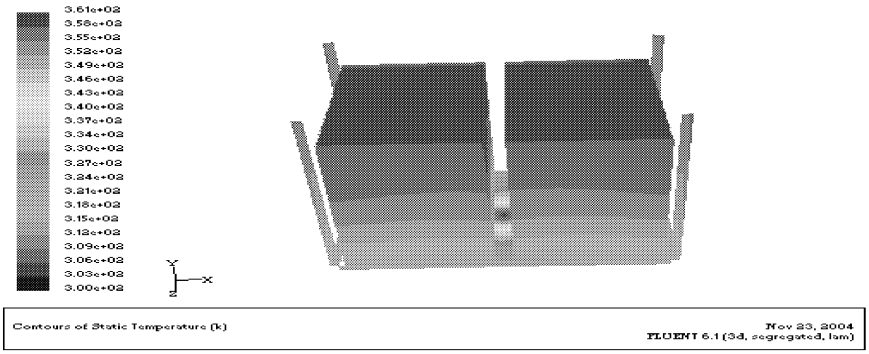

Figure7: (AL heatsink) heat flux 60w/cm2- flow velocity 10m/s

Maximum temperature of heat source is numerically accounted under the same flow condition and thermal load for copper which is about 88 ^{O}C (361K).

Cu heatsink

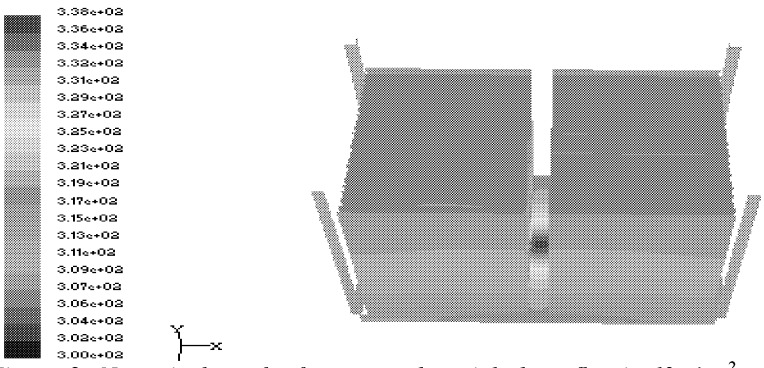

Figure 8: Numerical results for copper heatsink, heat flux is 60w/cm^2 and flow velocity is 10m/s. Maximum temperature of the source is about 65 ^{O}C (the scale of temperature at this figure is based on K)

The results obtained from numerical code indicate that the temperature of the heatsource is lower for copper approach at the constant power and flow rate. Maximum temperature of the heatsource is 338 K and 361K for copper and aluminum cooling devices respectively.

6.1 Theoretical and numerical thermal spreading resistance

One of the predominant parameters in the conduction heat transfer to the fins is the temperature difference (Δt) between the fin and base. Heat transfer rate (q) is calculated based on the largeness of (Δt); however there are other parameters that are also involved in determining of the heat transfer rate. The smaller temperature difference stands for lower energy transfer from the warm face to the fin. In this section the impact of the heat spreading (resistance) is studied by analytical and numerical calculations.

Figure 9 & 10 show the base section of two heat dissipation tools. In this case the applied power to both sinks is 60 W/cm^2 and flow velocity is 10 m/s. Thermal spreading resistance is a function of thermal conductivity, geometry and heat transfer coefficient. The geometry of the sources and sinks and flow rate are kept constant in this simulation so it is exclusively the thermal conductivity that varies and influence the heat spreading resistance.

As indicated in these figures more energy is conserved in centre of the base of aluminum pattern than the copper and this is due to the fact that energy transfer through the aluminum base is sluggish compared to copper. This can be expressed also by different thermal conductivities of copper and aluminum. Comparing the maximum temperature of two heat-ejector presented by contours (361 K and 338 K) establish the statements. The first result of numerical study is that more intensive hotspot is obtained for aluminum than for cooper. Since the heatsource is located at the centre so the idea is that to obtain a less intensive hotspot.
As we get further away from the centre of the base the temperature being lower for both aluminum and copper sinks. But the temperature at any certain point away from the centre is lower for Aluminum than the copper as shown in the contours of temperature. Consequently the aluminum fins that are placed away from centre of the base experience a lower (Δt) (Δt = temperature difference between base and fin of the heatsink) than the copper fins and this

stands for the fact that the aluminum fins gets a lower effectiveness than the copper. The justification of applying the fins (fin effectiveness) reduces if the heat transfer rate through the fin q_f decreases.

$$\varepsilon_f = \frac{q_f}{hA_{cb}\theta_b} \tag{56}$$

Aluminum heatsink: base

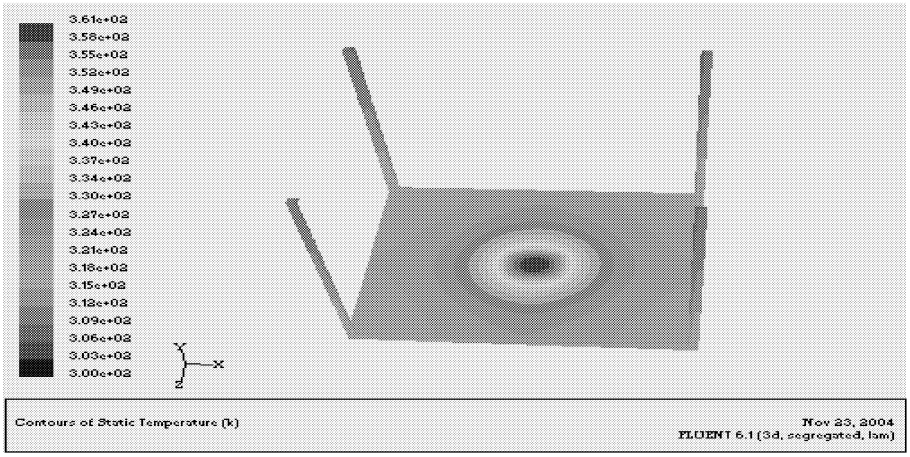

Figure 9: Heat spreading through the base of an Al heatsink: applied heat flux is 60w/cm^2 and flow velocity is 10m/s

Copper heatsink: base

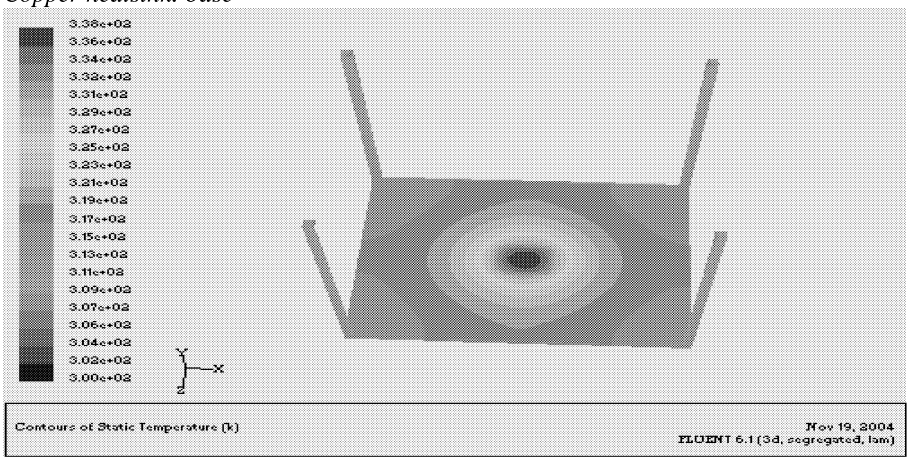

Figure10: Heat spreading through the base of a CU heatsink: applied heat flux is 60w/cm^2 and flow velocity is 10m/s

There are theoretical relations for accounting the total resistance based on heat spreading resistance that are assigned for different heat source and base configurations.
Here is presented two approaches of calculation of thermal resistance that are provided based on spreading resistance. [10], [2]

$R_{tot} = R_s + R_{1D}$ (57)

$R_{tot} = R_{sp} + R_{conv.}$ (58)

There is not essential difference between these two equations. Both assume that the total resistance is composed of three resistances:

$R_{tot} = R_{conduction} + R_{convection} + R_{spreading\ resistance}$

Dissimilarity arises from the difference temperature accounted in the correlations. They employ different terms to define the ΔT. The first relation defines R_{tot} by utilizing T_{mean} at both sink and source in the next expression: [10]

$R_{tot} = (T_{source} - T_{sink})/Q$ (59)

Where

T_{source} = mean temperature of the heat source (^oC)

T_{sink} = mean temperature of the sink (^oC)

Q = heat flow rate through the heat flux channel (W)

R_{1D} is a composed of one-dimensional convection and conduction thermal resistance.

$R_{1D} = (t_1 / k_1 + t_2 / k_2 + 1 / h) / A$ (60)

Where

t_1 and t_2 are thickness of the two-layer heat flux channel.

R_s is the thermal spreading resistance of the system. Thermal spreading resistance is a function of base and source geometry, thickness, thermal conductivity of the layers and heat transfer coefficient (h).

$R_s = f(t_1, t_2, k_1, k_2, h)$

The second interpretation of R_{tot} i.e. ($R_{tot} = R_{sp} + R_{conv}$) [2] utilizes T_{max} at the heat sink and combines conduction and spreading resistance in R_{sp} and separate convection resistance. [2]

$$R_{tot} = \frac{T_{max} - T_{REF}}{q} \quad (61)$$

q is heat transfer rate or power dissipation.

$$R_{conv} = \frac{1}{h_{eff} A_s} \quad (62)$$

Where A_s is the surface area of the plate or thermal spreader and h_{eff} is the effective heat transfer coefficient acting on the surface.

Lee et al [27] has developed a correlation for a circular plate with circular heating area. By these relations, the spreading resistance can be determined for two circular contacted area based on T_{max} at the heatsink. The dimensions and geometries are in accordance with figure 11.

$$\varepsilon = \frac{r_1}{r_2} \quad (63)$$

r_1 and r_2 are radios of the heat source and base, respectively, Se figure 11.

ε is a dimensionless quantity.

$$\tau = \frac{t}{r_2} \quad (64)$$

τ is also a dimensionless value that is defined in foregoing equation.

$$Bi = \frac{h_{eff} \times r_2}{k} \tag{65}$$

$$\lambda = \pi + \frac{1}{\varepsilon\sqrt{\pi}} \tag{66}$$

λ is another dimensionless parameter and is employed to determine the next dimensionless parameter.

$$\phi = \frac{\tanh(\lambda \times \tau) + \frac{\lambda}{Bi}}{1 + \frac{\lambda}{Bi}\tanh(\lambda \times \tau)} \tag{67}$$

$$\psi_{\max} = \frac{\varepsilon \times \tau}{\sqrt{\pi}} + \frac{1}{\sqrt{\pi}}(1-\varepsilon)\phi \tag{68}$$

In this relation $\psi_{\max}$ is a function of thermal conductivity of heat sink, geometry of sink/source and heat transfer coefficient on the heatsink (h_{eff}). [2]

$\psi_{\max}$ = f (Geometry $_{\text{sink/source,}}$ k $_{\text{sink}}$, h $_{\text{sink}}$,)

$$R_{sp} = \frac{\psi_{\max}}{k \times r_1\sqrt{\pi}} \tag{69}$$

The effect of convection process is involved in this equation in which gives the thermal conduction spreading resistance by using T $_{\max}$ at the sink.

Therefore, if the type of applied material in construction of the sink and source is held constant then the thermal spreading resistance is related to *cooling configuration that in turn impact the heat transfer coefficient,* thermal characteristics of the sink and geometry of the base and source.

To apply Lee solutions to other geometries, first one shall transform the considered geometry to circular form. Robert E Simons analyzed experimental Lee At Al relations for square geometry heat source and base and found that these formulas provide a reliable estimation of thermal spreading resistance. Relations and procedure to transform a square geometry to circular is presented in Fig. 11.

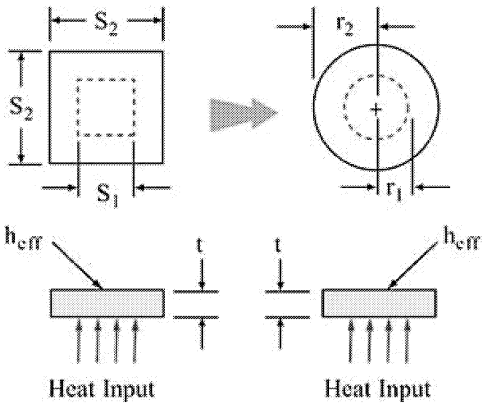

Figure 11: Geometry transformation from rectangular base to a circular case [2]

$$r_1 = \sqrt{\frac{s_1 \times s_1}{\pi}} \tag{70}$$

And

$$r_2 = \sqrt{\frac{s_2 \times s_2}{\pi}} \tag{71}$$

These equations can be employed for heat sinks with rectangular base and source. Further, the geometry transformation could be performed as follow:

$$r_2 = \sqrt{\frac{W \times L}{\pi}} \tag{72}$$

Where

W is the width of the heat source and L is the length of the base.

r_1 that is related to source is constant but r_2 have a new value because of the changes in sink geometry.

7. Manufacturing of the heatsinks

Production methods of cooling devices depend fundamentally on the type of the involved material in production. When aluminum is selected as the used material in construction of the cooling instruments then some types of manufacturing process exist that are compatible with the aluminum properties. Extrusion is one of the possible methods of aluminum heatsinks construction due to its softness. The extrusion term is usually applied to both the process, and the product obtained, when a hot cylindrical billet of aluminum is pushed through a shaped die (forward or direct extrusion, see Figure 12). The resulting section can be used in long lengths or cut into short parts for use in structures, vehicles or components. Other approaches are among the others, milling, die casting, cold forging. Die casting is a versatile process for producing engineered metal parts by forcing molten metal under high pressure into reusable steel molds. These molds, called dies, can be designed to produce complex shapes with a high degree of accuracy and repeatability. Forging is the term for shaping the metals by plastic deformation. It is distinguished from machining approaches that form the metals by drilling, sawing, milling, turning or grinding. Forging differs from casting in which the metal in its molten state is poured into a mold, whose form it retains on solidifying.

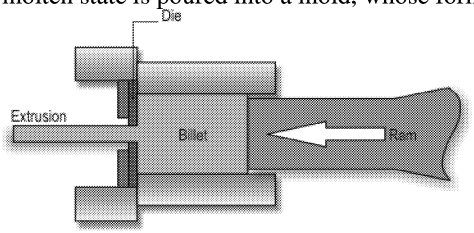

Figure12: Schematic of extrusion method

Copper heatsinks can be milled or deforms by die-cast method in very rough scales that are not practically applicable for heat-ejectors. The disadvantage of copper material is among the others, weight and cost. Density of pure copper and aluminum is respectively 8933 kg/m^3 and 2702 kg/m^3. If it was possible to make any copy of an aluminum heat removing tool by copper it would weight 3, 3 double as much as the typical aluminum. Heat transfer by conduction improves at thinner thickness of the base and larger surface area of the fins. This strategy agrees with miniaturization of copper heatsinks. Rough techniques such as die-cast and milling are not suitable for fabrication of miniaturized copper cooling devices. Employment of several thinner fins than a few thicker plates enhances the thermal characteristic of the cooling device. To compensate the heaviness of copper sinks applying the fins of 0, 2 mm thickness is proposed. Any technique such as casting methods, extrusion and milling has been failed for construction of copper cooling tools with 0, 2 mm plates. Shining property of copper made it difficult to take advantage of laser cutting method. Water cutting was also a rough technique to use for our purpose. The only remained alternative was making the copper heat-ejector by bonding the individual plates together under some mechanical operations. The suggestion made it possible to advantage the minor properties of copper in the construction of current cooling instruments by prior techniques and turn them to suitable characteristics of copper in making the cooling tools by mechanical approach. Shining of copper is not a drawback any longer when the new technique is substituted. Heaviness is solved by thinner plates and larger surface area is gained when using several thinner plates. The cost of construction drops also when the amount of consumed material is reduced in making the heatsink. The next step is designing the new copper pattern that is both the lighter and appropriate to the mechanical approaches. Even utilizing the brazing approach lied in our procedure because we had access to brazing furnace. The new designs were proposed and prototypes were made and prepared to experimental and numerical studies.

8. The proposed heatsinks and manufacturing factors

8.1 Fin selection

The introduced copper designs of cooling devices are associated with the type of the applied plates. So the fin selection constitutes an important element of our attempts. There are many considerations to choose a special extended surface configuration and it is a function of weight, space, manufacturing methods and cost.

8.2 Louvered fin heatsink

Normal and louvered fins are applied for copper designs and all of them are tested in the laboratory. The brazing technique is advantaged to make the louvered fin copper prototype. This case is much lighter than other sinks due to the thickness and the arranged louvered through the fin. A long louvered fin is rolled up and brazed in a pool shaped base. The fan is placed over the fins and is mounted on four columns. Impingement flow is suitable for this object in which the air is blowing downward to the fins. The air exits the fins through the louvers. The louvers penetrate to each others and there is no enough extent space between the loops. Different thermal capabilities gained for alternatives of louvered plates imply that there are still opportunities to improve the louvered sinks.

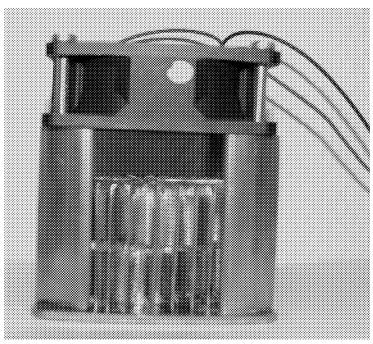

Figure 13: Louvered fin heatsink

8.3 Inclined free fins heatsink, SISE

The second variant is made of several flat plates that are bonded together. The thickness of the fins is 0, 2 mm. To reduce the roughness resistance, the bottom of the plates is polished to get a flat surface. The SISE fan mode is adopted for this offer. Arrangement of the fins of this model demands this mode of convection. The fins are inclined vertically manual. No brazing material is used for construction of this device.

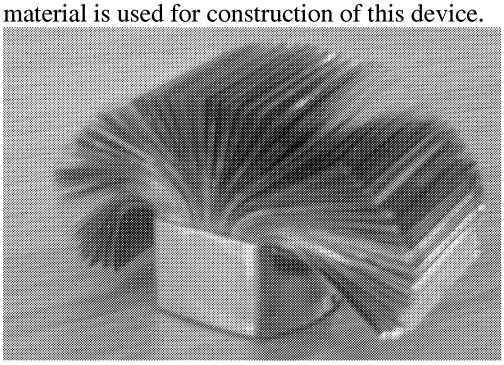

Figure 14: Inclined free fins heatsink (SISE)

8.4 Inclined free fins heatsink (TIBSE)

To avoid the drawbacks of the side inlet fan blowing a new design is proposed that is agree with the TISE mode of blowing. Horizontal rotation of the plates from zero to 180 degree with respect to the centre plate creates the spacing between them.

This heatsink is then optimized both in fluent environment and by other design considerations further to another model.

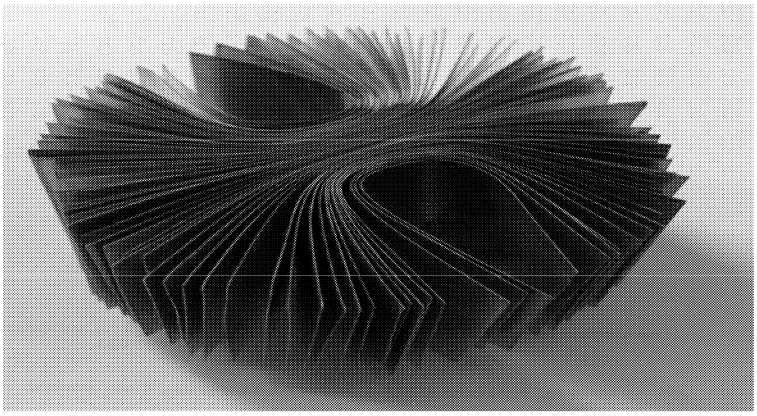

Figure 15: Inclined free fin TIBSE heatsink

8.5 Manufacturing considerations: Attachment and surface flatness

The rate of adhesive force of the heatsink to heat source even if a good sink is designed impacts the thermal performance of the cooling device. Case-sink connection creates a resistance that reduces the heat transfer between two surfaces. This resistance is affected by contact pressure, interface material and surfaces characterizations among others flatness (or roughness) and smoothness (or waviness). The cooling tools principally don't have a fixed performance because it can vary by contact resistance variation as well. Designers try to reduce the contact resistance by treatment of the base surface and applying the better thermal interface materials.

When attachment between the surface of the base and the heat source is considered, minimal air gaps between the surfaces have to be provided. Higher connection pressure lowers the air gaps between the surfaces and reduces the thermal resistance, because air has a low thermal conductivity than the metals applied in the heat-ejectors. Higher contact pressure is accomplished by employing the higher force on the surfaces as mach they can withstand. However, this application is limited by the cost and mechanical properties of the surfaces.

Roughness and flatness are due to surface quality i.e. coarsenesses and irregularities of surfaces. Achieving a quite flatness seems never being gained. Smoothness that is another surface property is determined by the waves on the surface.

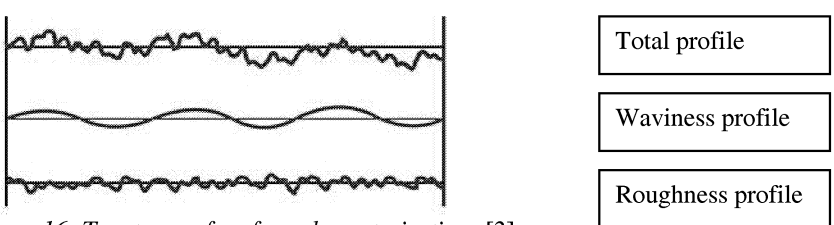

Figure 16: Two types of surface characterizations [3]

There are optical and mechanical methods to measure the smoothness of the surfaces. Average roughness R_a, root-mean-square roughness R_q, core roughness depth R_k and roughness kurtosis R_{ku} are four different parameters to determine the surface roughness. R_a and R_q are deviation types of parameters and their unit is of the type 1/ [length]. [3]

$$R_a = \frac{1}{l}\int_0^1 |y(x)|dx \tag{73}$$

$$R_q = \sqrt{\frac{1}{l}\int_0^l y^2(x)dx} \tag{74}$$

Where
y is a dimension vertical to the surface, and *l* is the length of the surface defined by x. The better flatness quality enhances heat dissipation and result in higher performance.
In order to have a good surface flatness and to avoid the waviness and roughness the prototype heatsinks are polished by the flat polish machine.

8.6 Optimized Inclined free fins heatsink, TIBSE

This sink is an improved prototype of the prior model. The weight is reduced by modifying the shape of the plates. To increase the heat transfer coefficient the number of plates is reduced. The inlet pressure drop is recovered by modifying the fin structure which results in a diminished flow bypass. Surface area is decreased but heat transfer coefficient is not exclusively depended on this variable but there are other factors that influence this parameter significantly. The advantages of these treatments are respectively decreasing the weight and recovery of the heat transfer coefficient. The thermal performance is enhanced as well.

Figure 17: Proposed modified prototype of inclined free fin heatsink

Further improvement of the design takes place under optimization in the fluent environment. Thickness of the plates is 0, 2 mm and the length is 92 mm. the fin design is shown in figure 17. Although all the experiments carried out by this pattern but to avoid using any screw or cover around the fins a new base is proposed. A copper plate with a hole in the centre is proposed and the dimension of the centre hole is as much as the dimension of bottom of bounded fins. An advantage of these designs is that a direct contact between the fins and heatsource is established which eliminates the thermal resistance between the base and the fins. The weight of the offer sink is about 200 gram but this weight is further reduced under

optimization in the fluent. No experimental effort, numerical simulation and optimization are performed respect to the fins holder.

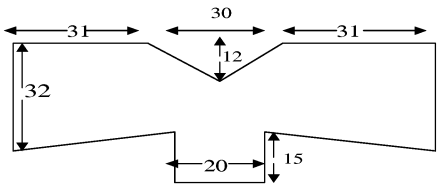

Figure18: Dimension of the applied fin in the heatsink is shown in this figure

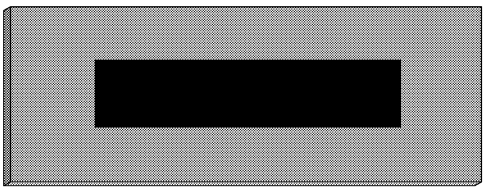

Figure 19: The base (fins holder)

8.7 Flat free fins heatsink, TISE

The structure of this design is based on the mechanical principles assigned for previous copper cooling instruments introduced above. All of these copper cases include the fins that are composed of two parts i.e. foot and overhead. The foot part has direct contact with the heatsource. Construction of this heat-ejector can be simpler than earlier models presented previously from manufacturing aspects. This sink is developed by CFD as well as design considerations for mechanical fabrication of copper heat removing tools and it is composed of a perforated base (fins holder) and 70 fins.

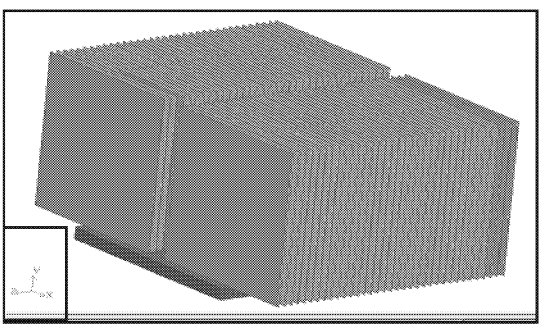

Figure20: The proposed flat free fins heatsink

Dimensions of the employed left and right fins in this sink are introduced in figure below.

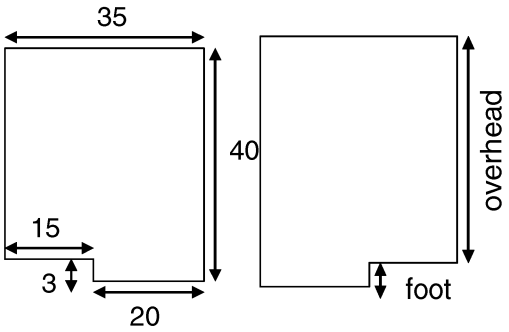

Figure 21: The dimension of the suggested fins for above design

8.8 Base or fins-holder

The selected base or fins-holder is an incorporated copper plate with 3mm thickness. The gaps of the base are about 0, 2 mm or a little bigger than the thickness of the employed fins. The interval between the gaps can be 1 to 2 mm. Foots of the fins are inserted in the gaps of the base. Two ways are proposed to keep the fins stable in the base. Soldering is the first suggestion. Upper face of the base may be soldered to the fins to hold them firm together. Another alternative is dipping the fins in the brazing material and braze them in the furnace. Both SISE and TISE mode of forced convection are suitable for this model but TISE that is more capable adopted for heat removal by convection. The fan blow perpendicular to the base which results in the boundary layer gets thinner compared to horizontal blowing.

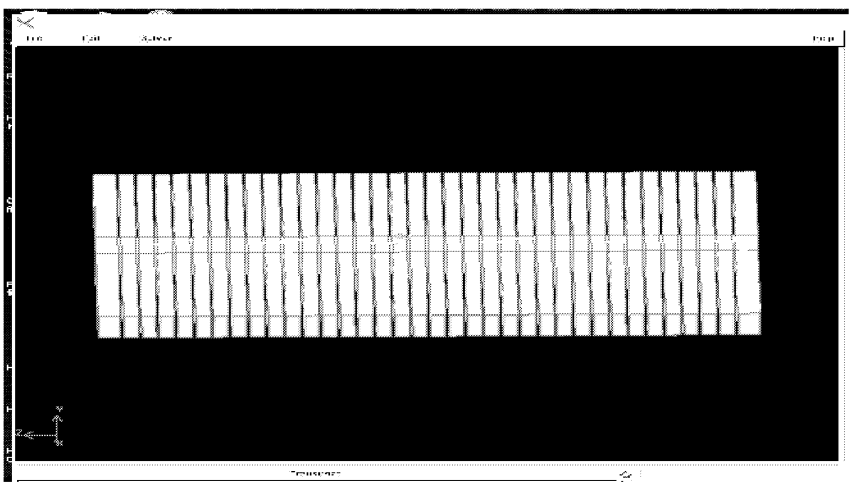

Figure 22: The base or fins holder proposed for above copper heatsink

9. Experimental set up

A series of experiments are performed in order to evaluate the samples and to have a good judgment about them. They not only are put to the test but also compared to current aluminum heatsinks. A number of aluminum heat-ejectors are adopted and their performance is measured experimentally. In the next step the copper prototypes are tested and compared to the best aluminum samples resulted from the first experimental efforts. The test of the copper examples takes place at the same experimental condition as for aluminum.
The fan used for characterization of the samples is A0812MS-A70GL with the following specifications: DC 12V, 0,15 A, 80×80×25, 1,8 W, volumetric flow rate 31,4CFM. The same fan is used for both samples.
The temperature is measured by data acquisition 34970A in associated with HP Bench Link program. The adhesive "k" type thermocouple is applied to measure the temperature of the fins and heat source. A 1400 W, SM3540 power supply in the range of 35V × 40A is adopted to run the resistors with different current. The heat sources are respectively 25, 30, 100 and 100-200 watt resistors of the type Mp725 (A = 0, 67 cm^2, 1.00 & 1% R) and MP930 (R=1, A= 1, 5 cm^2), MP9100 (R=1, A= 3cm^2), Fabr Arcol [2, 2 Ω, A= 9,9cm2 dimension: 3,8 ×2,6cm). The heat is generated in a resistor that serves as a heat source. Resistor is attached to bottom of the heatsink. None silicone heat transfer compound (HTC) is used to improve attachment between the heatsource and heatsink.

Thermal performance is determined by using the initial (room temperature) and maximum temperature of the heat source or the equilibrium temperature at the applied power.

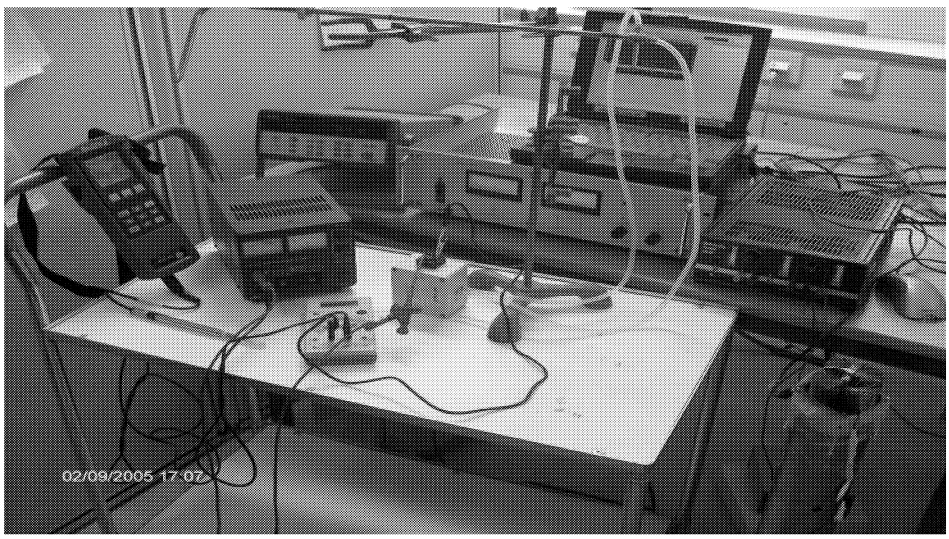

Fig.23 Measurement equipments

Different powers are applied to the source and equilibrium or maximum temperature of the source is measured.

10. Experimental results and calculations

Before presenting the results it is worthy to define a variable that is computed in the results. This variable is performance that represents the thermal dissipation capability of the heatsink.

10.1 Relative performance

"Relative" in this context implies that performance of a heatsink is not an absolute character and depends on heat flux and not just heat rate in the source.

The cooling performance of the heatsink is estimated by its heat dissipation rate for a given inlet velocity and heat flux. Maximum temperature of the source is a criterion for cooling performance of the sink and that is why this variable is applied in the correlation used for determining of the cooling performance.

$$MaxT_{sou} = T_r + (p_e)(P) \tag{75}$$

There are many ways to evaluate the thermal properties of the heatsinks. One of these ways is based on the thermal resistance that is a property of them and is a criterion for measuring the performance of a heatsink. If we assume that thermal resistance of a heatsink is 2 ^{o}C per watt (°C/W) this means that the temperature of the apparatus and not heatsink raises 2 ^{o}C per watt if the heatsink applies to cool the apparatus. When comparing the cooling devices, by assuming that the other factors like cost and weight are constant for all of them, the best way is determining the lowest thermal resistance of considered sinks.

It has to be noted that thermal resistance is not the exclusive way in defining the thermal identification of the heatsink.

Another way to specify the thermal identity of different types of heat-ejectors is to measure the maximum temperature rise of the patterns (or base) against the pressure drop or inlet air velocity.

For a single heatsink combined with a fan, pressure drop versus fan rotational speed can be a criterion in determining of the performance of the heatsink.

Width of the heatsinks perpendicular or parallel to airflow has a great role in the design and performance. But the *length of the fins* has lower role in this concern. Width of the heatsinks is related to fin spacing, fin thickness and number of fins. The width is linearly proportional to performance. But the square root of the fin length is proportional to performance. Duplication of the width of the heatsink causes double heat dissipation but twice increasing in the length of the fins only give rise to an 1.4 times enhancement of the thermal performance.

The vendors publish the performance graph for the heatsinks but as mentioned above, external condition of the heatsink affect the performance and that's why these graphs consist of two plot specified for natural and force convection. The curve for force convection is a plot of required (heatsinks) thermal resistance ($R_{s\,a}$) versus minimum air velocity. Since in this case, T_{sa} is linearly proportional to Q therefore R_{sa} is independent of Q. The natural convection curve represents the sinks temperature rise, T_{sa}, versus Q.

Heat transfer rate can be determined by the amount of flow through the cooling device. Heatsinks configurations have various flow resistances that cause a portion of the entering flow spreads to other direction i.e. top and sides than through the fins. Thus the ratio of the amount of leaving air through the back of the heatsink to the amount of entering air can serves as heatsink performance.

We employed the correlation (75) to compare the performance of the samples under the same conditions.

In this equation the computed performance provides a measure of the temperature rise in the heatsource per unit power. As the quantity of the accounted performance is lower the thermal

dissipation capability of the heatsink is higher because this value is accounted based on increasing of temperature of the heatsource.

10.2 Coolant temperature

Room temperature is also a decisive factor in determining the thermal capability of the heatsinks. Surrounding temperature is actually the fan blowing temperature that is accounted as the inlet fluid temperature to the heatsink. It is obviously that the cooling is more effective when the fan inlet temperature is lower. The experiments are tried to be conducted at constant coolant temperature that is why when comparison is intended the aluminum and copper experiments are carried out at short time intervals to avoid variation of room temperature. According to the equation below at lower environment temperature the surface temperature decreases if other parameters are kept constant.

$$T_S = T_\infty + \frac{q}{hA} \tag{76}$$

10.3 Temperature of the Al and Cu heatsinks

In the foregoing relationship assigned for determining the heat characteristic of cooling instruments, the heatsource temperature involved in the equation but not the sink temperature because the heat-ejectors are large enough to have a temperature distribution through them but heat sources are so small that we can consider a lump temperature for them. Assigning a location in the heatsink representing the sink temperature is not possible because of the extent temperature distribution inside it.

1- Aluminum heatsinks

Heatsink	Coolant temp.	Heatsource temp. (^{0}C)	Performance (^{0}C/watt)	Power (W)	Heatsource type 100-200W A=9,9cm^2	q" W/cm^2	Max q (W)
AL (38 fin)-blue	23	44	0.42	50	Arcol , 100-200W	≈5	147
AL (96 pin fin-yellow)	22	57	0.7	50	Arcol , 100-200W	≈5	88
AL (120 pin fin)	23	42	0.38	50	Arcol , 100-200W	≈5	163
AL (cast)	23.5	41	0.35	50	Arcol , 100-200W	≈5	177

Table 1: Experimental results obtained for aluminum heatsinks

2- Copper heatsinks

Several prototype copper heatsinks are built and tested at the first stage.

Copper heatsinks	Coolant temp.	Heatsource temp. (^{0}C)	Performance (^{0}C/W)	Power (W)	Heatsource type	Max q (W)
Brazed-louvered fin	23	62	0,78	50	Arcol 100-200 W	80
SISE fin	26	62	0,72	50	Arcol 100-200 W	86
Shorter brazed louvered fin	23,5	55	0,63	50	Arcol 100-200 W	98
Single brazed fin	23	50	0,54	50	Arcol 100-200 W	115

Table 2: Thermal experimental results obtained for copper heatsinks

The thermal behavior of these samples is studied. Performance of copper heatsink is measured and results are presented in table 2.
The drawbacks of these copper patterns are considered and a new design shown in figure 17 is proposed.
The best aluminum heatsink is selected and compared with the new copper sink. An intensive heatsource is adopted for both samples. A variety of powers are imposed to sources and equilibrium temperature is measured for every case. Heat flux is also reported in the table that is accounted based on the cross section area of the source and applied power.

q (W)	**A_{source}= 0,67cm^2** q'' **(W/cm^2)**	**T_{max}** copper	**T_{max}** Aluminum
5	**7,46**	**31,8**	**33,9**
10,5	**15,67**	**44,6**	**47,3**
14	**20,89**	**52**	**55,9**
22,5	**33,58**	**70,3**	**78,3**

Table3: Thermal experimental results of copper and aluminum heatsink

The results are shown on the next graph when a heatsource of type MP725 adapted to the both aluminum and copper examples.

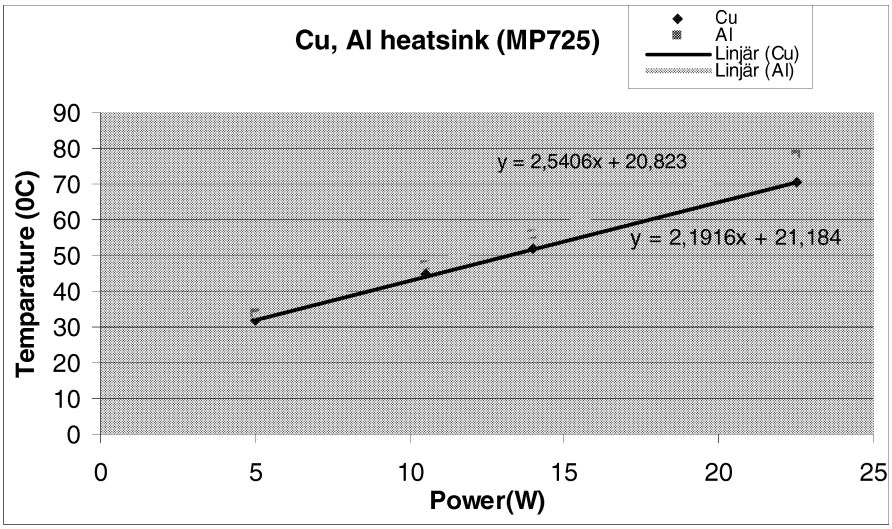

Figure 24: Comparison of thermal characteristic of aluminum and copper heatsinks (heatsource of type MP725 is applied)

Thermal performance value is accounted 2, 19 ^{0}C/W for copper and 2, 54 0C/W for aluminum.
The graphical presentation of the experimental results obtained for the second source MP930 is displayed in the next graph.

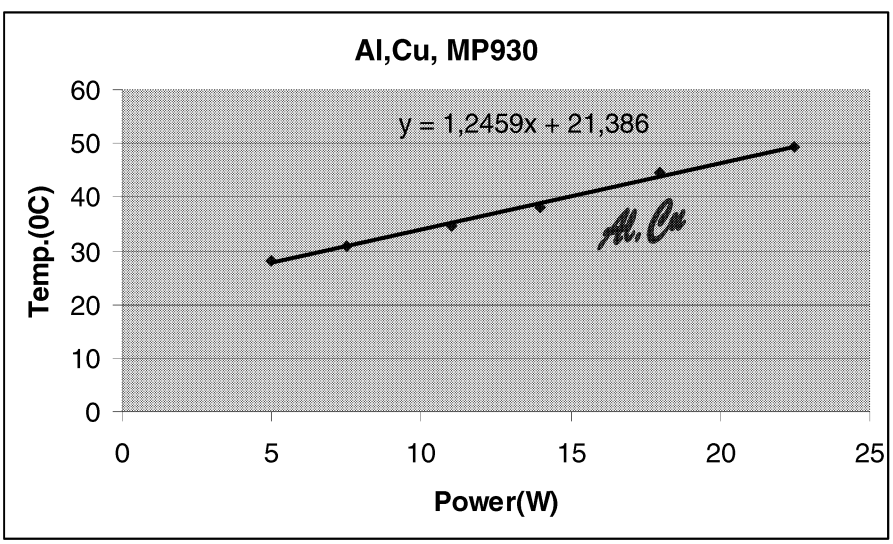

Figure 25: Comparison of thermal characteristic of aluminum and copper heatsinks (heatsource of type MP930 is applied)

The same results are gained when testing the bigger heatsource of type MP930. The accounted performance for both aluminum and copper sink is 1, 24 ^{0}C/W.

11. Numerical, optimization, and scaling up results of inclined free fins

11.1Predicted relative numerical performance

The proposed heatsink is modeled three dimensional in the Gambit and is simulated in the fluent. Some approximations related to curvature angle of fins that do not fundamentally impact the results are performed for simulation ease. Thickness of the different sections, applied material, number of fins, and the total shape of the numerical model accord with prototype. The heatsink model used in numerical calculations is shown in figure 26.

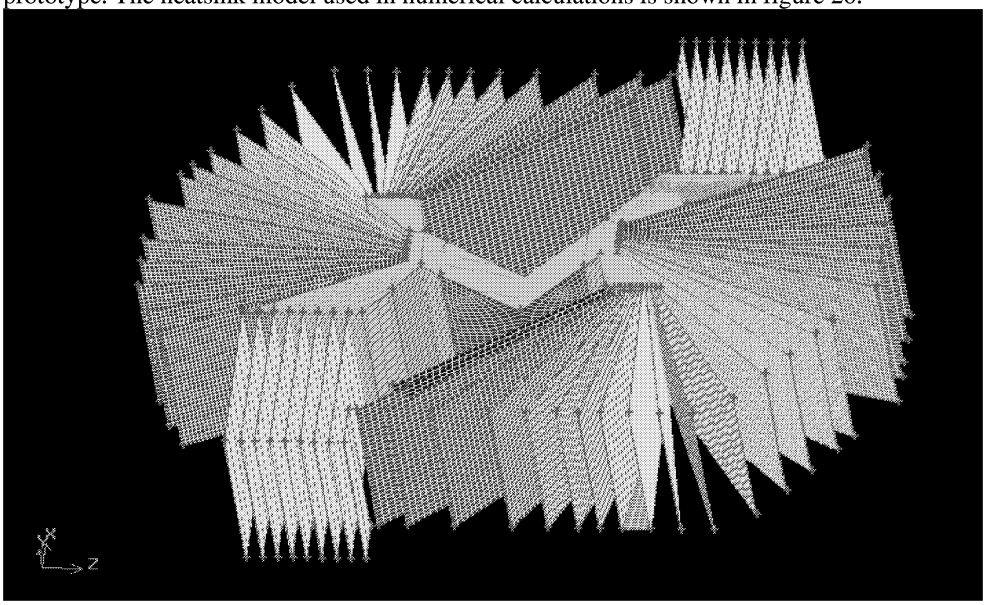

Figure26: The inclined free fins heatsink modeled by Gambit analogous the experimental model (the grid is meshed here)

The thermal dissipation capability of the proposed heatsinks is theoretically accounted for by means of the obtained results from the numerical solutions and equation (75). The adopted initial or environmental temperature of the samples under simulation is 296 K. Further optimizations are also carried out to modify the proposed model.

Simulations are accomplished under laminar and turbulent flow but there is no significant departure between the results. This can be due to a poor turbulent behavior of the flow in the channels. It is noteworthy that we do not claim that the quantitative results of CFD simulation represent the ultimate flow and thermal identity values of the fabric patterns. And maybe the numerical models do not match exactly the experimental patterns as well.

But the simulation measurements in our task primarily serve as a reliable tool for qualitative comparison of aluminum and copper heatsinks, thermal and flow behavior thorough the channels, and for optimization goals. The quantitative results of modeling are able to represent the thermal characteristics of manufacture models relatively and not absolutely.

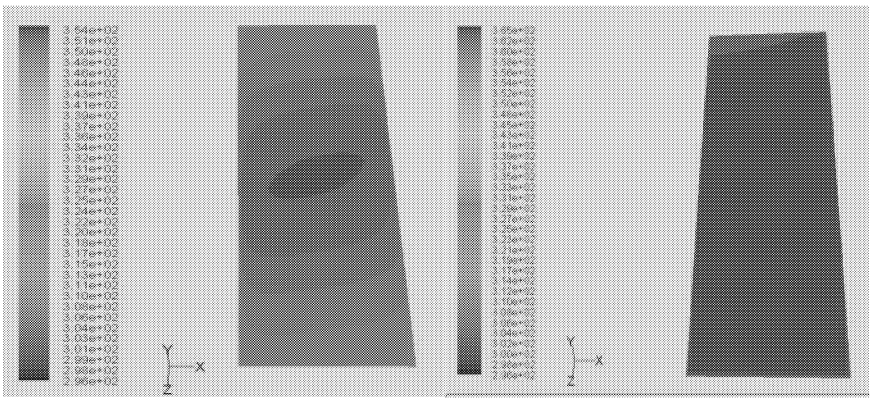

Figure 27: Heatsource temperature of 12mm fin foot
Figure 28: Source temp. of 5 mm fin foot

11.2 Thermal dissipation capability

The model is also scaled up by CFD code for other applications such as servers that do not demand severe limitations for largeness or heaviness of sinks. A 40 percent three dimensional up scaling is conducted by CFD. It is obviously that the weight of the sink and thickness of the fins increases by up scaling but the performance of the sink improves considerably as well.
The results of the primary simulation, optimizations and scaling are presented in table (4).

Fin foot length (mm)→	12	5	3	3(40% scale up)
Power (W)	117	117	117	230
T_{max} (^{0}C)	365	354	346	337
Pe (^{0}C/W)	0.59	0.49	0.42	0.18
Flux(W/m^2)	700000	700000	700000	700000

Table 4: Performance of the model under primary condition, optimization and scaling

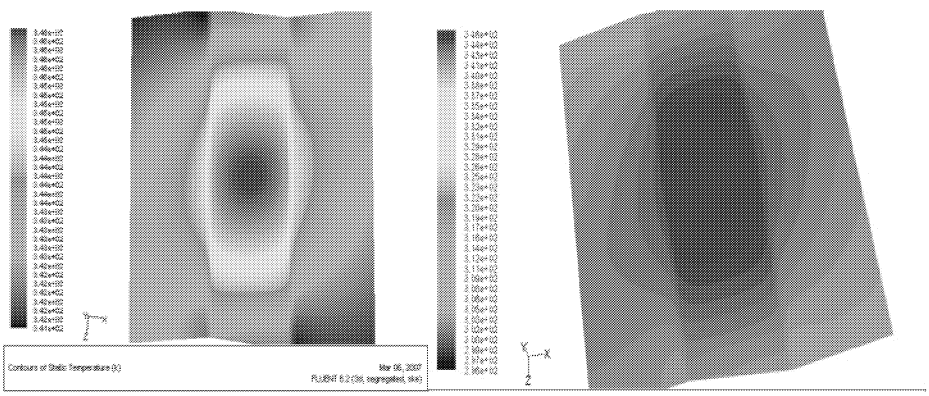

Figure 29: Heat source temperature of the 40 % scaled up of 3mm fin foot sink
Figure 30: Heatsource temperature of 3 mm fin foot heatsink

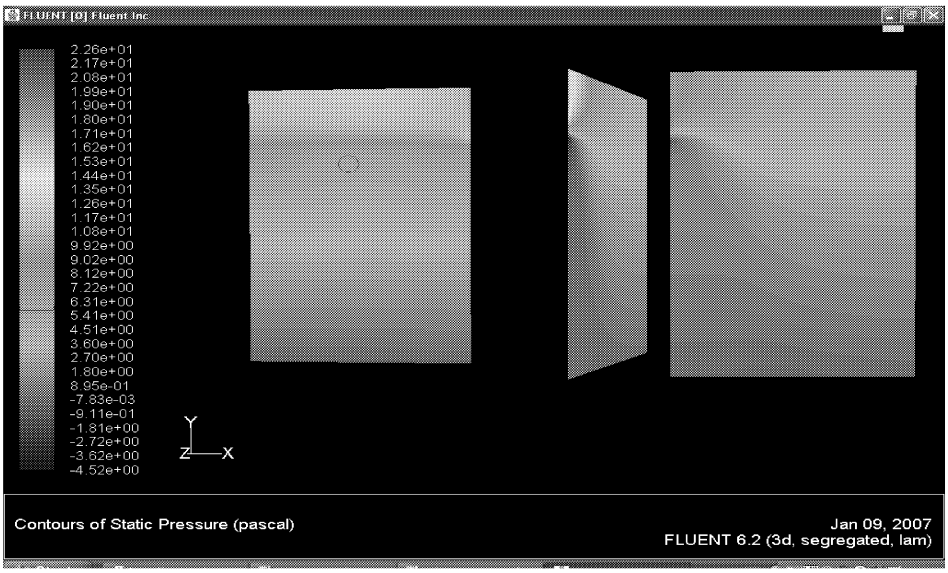

Figure31: Static pressure- airflow between 3 plates

12. Numerical results obtained for flat free fins heatsink

12.1 Heat flux and total cross section area of heatsource

The heatsource includes three zones in the simulated heatsink and the same heat flux exerted to the source zones.

Area	(m2)
heatsource1	0.00027500003
heatsource2	0.0018500002
heatsource2:019	0.00034999997
Net (Area)	0.0024750002

Heat flux adapted to Heatsource zones in simulation

q"= 100000 W/m^2 (10 W/cm^2)

Net heat transfer rate:

Zone 9 (heatsource1): 27.500395
Zone 8 (heatsource2): 184.97778
Zone 19 (heatsource2:019): 35.000668
Net heat-transfer: 247.47885

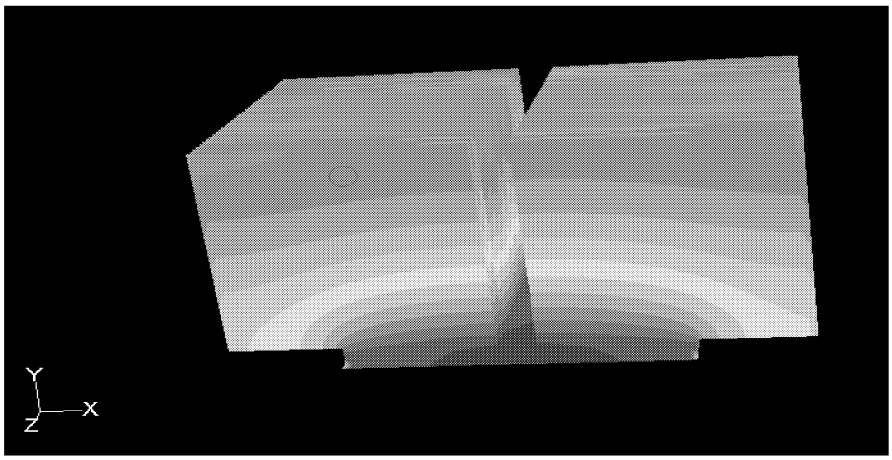

Figure32: Presentation of position of the source, fins and base to each other and energy distribution through the heatsink modeled in the gambit and simulated by CFD

12.2 Thermal characteristic of flat free fin TISE

The maximum temperature is always observed in the heatsource and as it has been shown in the numerical calculation, this temperature under the mentioned conditions is about 80 0C which is shown in the figure 33.

Maximum temperature of the source observed from the fluent, supplied power and initial temperature are the variables of the performance equation.

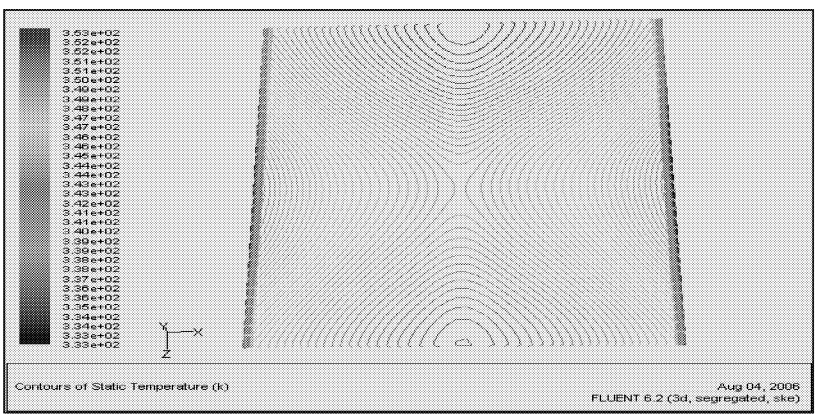

Figure33: Temperature distribution on the heatsource of the flat free fins

The thermal dissipation capacity of the proposed heatsink may be computed as following:

$T_{max} = T_{initial} + (Per. \times q)$ $\quad 80 = 23 + Per. \times 247$

$Per. = 0, 23\ ^{o}C/W$

Maximum heat transfer rate

If we suppose the ultimate possible temperature of the source is 90 ^{0}C in a computer so the maximum power may be applied at a rate of 100000 W/m2 can be 290 W when this heatsink is operated.
90 = 23 + 0, 23× X

q_{Max} = 290 W

12.3 Hydraulic characterization of the flat free fins

Fin density, Flow bypass and pressure drop are related closely to each other when treating the hydraulic behavior of the heatsink. Pressure drop and flow bypass may be treated by modifying the variables such as fin density. Fin density defines as the total thickness of fins per width of the heatsink and it is the space that fins occupied across the heatsink. Fin density equation: [5]

$$D = N\frac{t}{w} = 1 - (N-1)\frac{s}{w} \tag{77}$$

The next correlation describes the fin density for circular pins [4]

$$D = n^2 \frac{\pi}{4}\left(\frac{d}{L}\right)^2 \tag{78}$$

Where
L= length of the heatsink, edge length
n= number of pins or fins
d= pin diameter

The fins are like the obstructers placed in the path of the flow and resist to air stream through the fins. Thus increasing the fin density will enhance the contraction losses through the heatsink and therefore the fluid tends to flow to lateral and top of the heatsink (tip gaps) that induce a lower pressure drop. The pressure drop is generated due to the wall shear stress produced between the solid surface and the fluid. The acceleration losses are generated when the flow cross-section at the entrance of the heatsink changes suddenly. Acceleration factor is defined in equation (13). On the other hand heat-ejectors are usually placed into a duct and the fan is mounted over or at the side of the duct. Spaces between fins have more flow resistance than surrounding duct and hence the air tends to flow around the heat sink and not between the fins and thus air velocity between fins becomes lower than through the fins.
Some times the flow bypass at longitudinal cooling instruments reaches up to 60% which significantly diminishes the overall heat transfer rate through the fins and consequently the heat transfer coefficient.
Pressure drop is computed by observing and analyzing the static pressure distribution. The air flow is modeled by CFD code. The numerical results turn out that the pressure drops lies in a range of 4-6 Pascal in most of the zones of the heatsink. The contour of the static pressure is shown in the next figure.

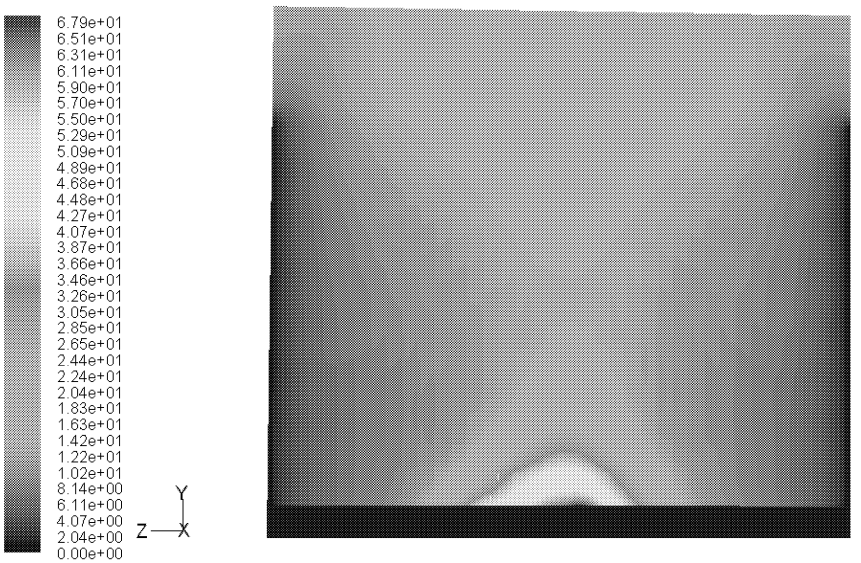

Figure 34: Static pressure distributions in the channel at the middle of heatsink

13. Discussion

13.1 Inclined free fins heatsink

The size of the heatsource has a crucial effect on determining the thermal identity of the heatsinks. If the cross section area of heatsource does not take into account the calculated performance of the sink is not reliable. That is way the intensity of heat or heat flux should be noted when measuring the performance. The heat flux is proportional to cross section area of the source. Cooling devices have different response to different fluxes at the constant power. In all of our experiments conducted to determine the characteristics of the samples, the heat fluxes or cross section area of the sources are expressed. A relative performance is defined to evaluate the thermal behavior of the models.

	Heat source	*T/q* ($^oc/w$)	*A surface area* (m^2)	*heatsink*	*h* (W/m^2k)
1	*MP725*	*2,25*	*13,9E-02*	*Al*	*3,3*
2	*MP930*	*1,25*	*13,9E-02*	*Al*	*5,76*
3	*MP100*	*0,8*	*13,9E-02*	*Al*	*9,1*
4	*Arcol (100-200)*	*0,33*	*13,9E-02*	*Al*	*21,6*

Table5: Thermal performance and heat transfer coefficient obtained at different fluxes

The thermal characteristic of copper samples is not evaluated absolutely but they are compared to standard current references to account the relative value. However not only the references are compared together but also heat fluxes are expressed under the experiments. Although we have measured a relative performance but since they are compared to standard references so the relativity of the calculations approaches an absolute assess.

As it is indicated in figure 24 two graphs are not parallel but there is a divergence between them that is proportional to the applied power. At higher temperature the divergence increases that indicates the copper type is more capable when the sources are smaller and more intensive. So the copper cooling tools have better capability in accordance with the miniaturization of sources. This can be due to better conduction inside the copper material and lower heat spreading resistance through them. This effect reduces either when sources are larger or lower intensity is applied and therefore the angle between two graphs reduces. The experiments agree with these statements when a larger.
Shorter brazed fin that tested had a base with 6mm thickness that could deteriorate the thermal behavior of the heatsink. Decreasing the thickness up to 2mm can further improve the performance.

13.2 Heatsink optimization

With composite systems it is convenient to work with an overall heat transfer coefficient, U. The overall heat transfer by combined conduction and convection is frequently expressed in terms of an overall heat transfer coefficient, U. The next expression is defined according to Newton's law of cooling.

$$q_x \equiv UA\Delta T \tag{79}$$

Where ΔT is the overall temperature difference.

The optimal UA-product for manufacturer is its maximum value with respect to the limiting factors such as cost and volume of the heatsink.

To attain this goal, the optimal fin configuration i.e. fin density and fin geometry have to be considered because fin density is inversely proportional to U but directly proportional to A. Decreasing the fin density (D) reduces the heat transfer surface area, A, while the flow rate through the fin array increases in which tends to enhance the U. But a higher fin density gives rise to lower U and larger surface area.
That's why designer have to obtain maximum UA-product by optimal fin configuration.
Weight, thickness, geometry, volume of the models, heat transfer coefficient, fin spacing, number of the fins, are among other things the optimization variables which takes into account. Some of these factors are considered from manufacturing point of view and others are related to applications concern and quality or characteristic of the component.
Maintaining a balance between the manufacturing variables, application factors and optimum thermal characteristics of the proposed model is intended when designing a heatsink. Some variables are improved independent of the numerical computations by observations, experiments and theoretical analyses.
Optimization in the fluent is essentially conducted by decreasing the fin foot length while other variables such as air velocity and air temperature are held constant.
The prototype is made with a long fin foot length for ease of fabrication. This length is treated as a variable in optimization efforts in the CFD to improve the model.
Extension the surface area is desirable but it does not result in the better heat transfer coefficient. Even decreasing the surface area may elevate the thermal performance of the heat sink. Other relevant parameters than the heat transfer coefficient may be degraded by increasing the surface area which are significant in fabrication considerations. Comparing the primary and optimized design of this heat sink turns out that the weight, fin spacing, heat transfer coefficient, and heat properties of the heat sink are improved. Some times it does not observe any improvement when changing a variable in some extent and this is due to a conversely relationship between some parameters which are decisive in the thermal capacity of the sink.

13.3 The fins holder

From the design point of view the cross section area of the fins-holder plate (figure 9) should be wider than the heatsource, in this case the convective heat transfer coefficient enhances. Otherwise, the heat transfer coefficient degrades due to the fact that exclusively the thickness (Δx) increases and surface area remains constant. In the other words the thermal resistance between the fins-holder and source increases and consequently the thermal performance of the inclined free fins diminishes.

13.4 Modeling the air flow through the fins

In addition to the temperature other physical quantities such as flow velocity, dynamic pressure, and static pressure are also predicted by CFD code for this heatsink. Due to relevance of the pressure drop in cooling management, this element is accounted to evaluate the thermal parameters. Any assessment of the model may not be fulfilled without considering the pressure drop.

High pressure drops between the sink and the fan are indications to some defects in the design and may be adjusted by modifying the model. This type of pressure drops is associated to the geometrical considerations and tends to intensify the flow bypass.

High values of this parameter may degrade the heat transfer coefficient and result in a poor cooling characteristic of heatsink. On the other hand pressure drop contributes the heat transfer coefficient and improve it.
Gneilinsky [14] is developed a formula (equation 33) for internal flows representing relationship between friction factor obtained from Moody diagram and Nusselt number.

$$Nu_D = \frac{(f/2)(\mathrm{Re}_D - 10^3)\,\mathrm{Pr}}{1 + 12.7(f/2)^{1/2}(\mathrm{Pr}^{2/3} - 1)}$$

According to this equation the dimensionless pressure drop represented by friction factor accompany the heat transfer coefficient.
Pressure drop is accounted by measuring the difference of inlet and outlet static pressures in the channels. A moderate pressure drop indicates appropriate fin spacing and fin numbers. Pressure drop at some locations of channels is accounted between 4-6 Pascal that is not so large. It is not either desirable driving the low pressure drop internal flow in the channels.
Heat sinks are not the closed systems in respect to their periphery boundaries and it is hard to assign single inlet and outlet flows for them. Due to existence of more than one outflow from the channels there is static pressure distribution at all directions and this can make the interpretation of pressure drops more complicated.
Unequal inlet pressure at some channels may be due to the reversal flows at entrances. The amount of reverse flow is directly proportional to number of the fins, thickness and may be other obstacles like the presence of a core in the design.
The flow behavior through the heatsink is also taken into account by comparing the dynamic pressure and flow velocity distribution.
These two parameters introduce the same patterns of distributions although they possess different amounts. This means that the two parameters are directly proportional to each other. Comparison of these factors by CFD code at the same three locations in the heatsink is shown in figure 35. The trends are the same but the contours are representative of different quantities.

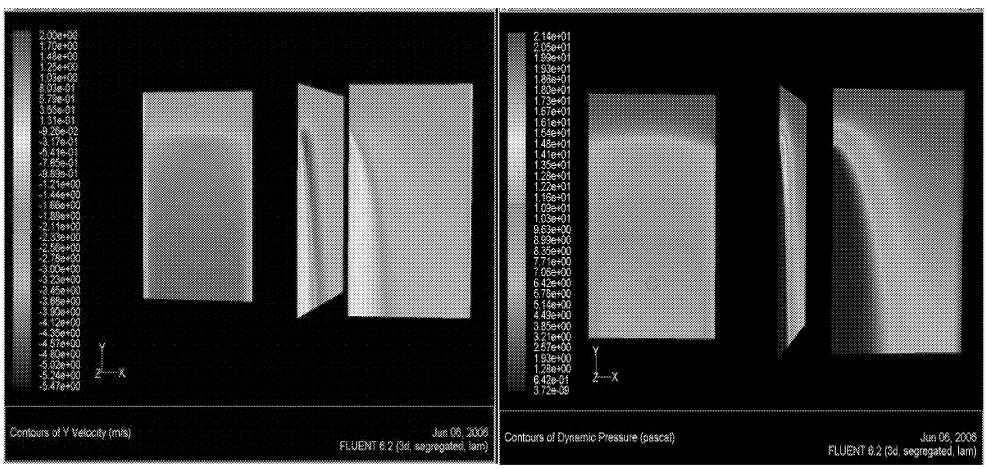

Figure 35: Comparison of flow velocity in y direction with the dynamic pressure

13.5 Flat free fins heatsink:

Heat transfer coefficient, Flow bypass and pressure drop

As noted in the preceding section the dynamic pressure and vertical component of flow velocity have the same distribution however they pose different quantities. This relationship can be shown for this heatsink schematically in the figure (36).

Heat transfer coefficient drops steadily from upstream to the downstream which is due to collision of the fluid particles to the base and consequently production of fluid circulation. A reversible flow is produced at the bottom of the heatsink which tends to flow upward and toward the outlets. The collision of downward and upward flow particles decelerates the downward flow velocity as shown in figure (36) which degrades the heat transfer coefficient downward. This is another scenario of fluid velocity than for preceding heatsink. The difference arises from the lack of the base at bottom of that heatsink which result in the increasing of flow velocity steadily downward as shown in the figure (35).

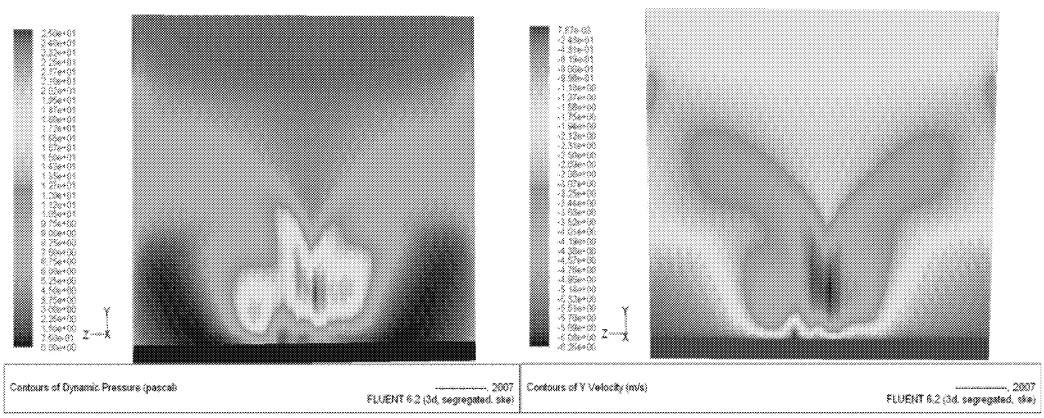

Figure 36: Comparisons of the contours of dynamic pressure and the vertical component of flow velocity

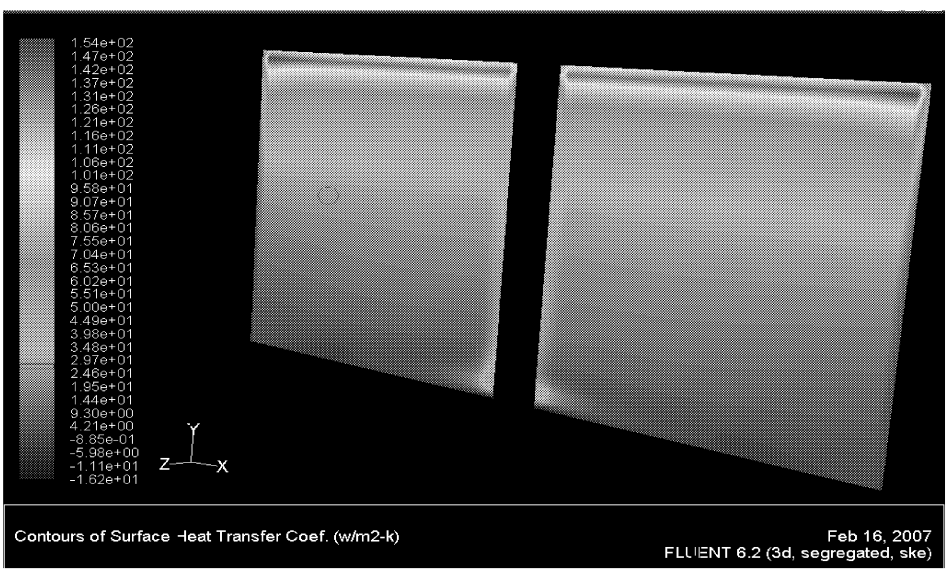

Figure37: Local heat transfer coefficient

Heat transfer coefficient for cooling devices including more fin number should be higher than for those with fewer plates. This can be due to the increased surface area. Flow bypass affects the heat transfer coefficient and tends to decrease it.

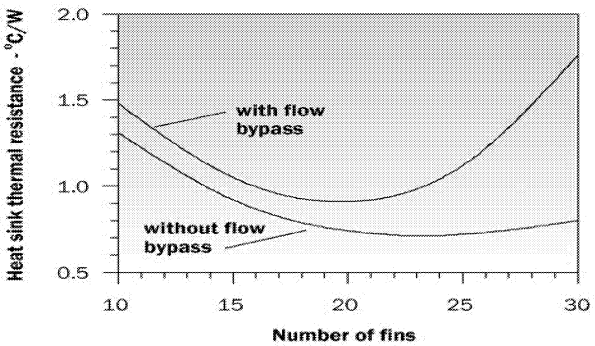

Figure 38: Number of fins versus thermal resistance [8]

Extending the surface area should result in the improvement of the heat transfer rate but due to the flow bypass effect; this object is not entirely obtainable. By increasing the surface area, lower fin spacing is provided which in turn increases the pressure drop through the fins and consequently, higher flow by pass is resulted. Increasing the clearance tends to intensify the flow bypass. It is worthwhile to note that flow bypass is not zero for zero tip clearance because of the lateral clearance. Fin number is associated with the total pressure drop and flow bypass.

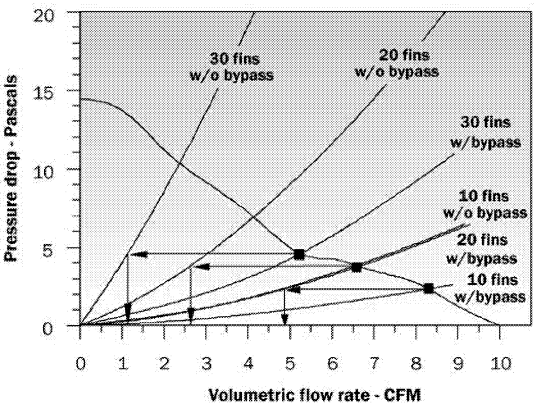

Figure39: Volumetric flow rate versus pressure drop [8]

The static pressure is modeled through the fins and it is computed numerically. In some locations of channels the static pressure is increased this can be due to either decreasing the dynamic pressure at this regions which occur at stagnation points, or resulted from interaction and mixing the streams from neighboring channels. Streams with higher pressure are transferred to the adjacent channels with lower pressure and exert an external force to these streams that give rise to the momentum transport to these zones.
Mixing, exiting and entering the flows, at unpredicted locations in multi channel heatsinks provide a more complicated view of variation of parameters through the heatsink.

13.6 Thermal boundary layer ($\frac{\partial T}{\partial z}$), versus velocity boundary layer ($\frac{\partial V_y}{\partial z}$),

Velocity boundary layer is the region of fluid flow adjacent to the surface of a solid that velocity is reduced under the impact of the viscosity.

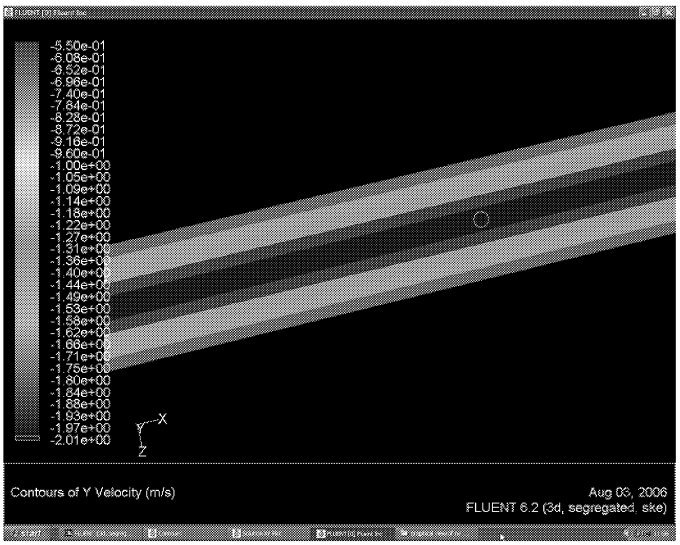

Figure 40: Demonstration of velocity boundary layer between the fins ($\frac{\partial V_y}{\partial z}$).

Thermal boundary layer is the region where temperature gradients are present in the flow.

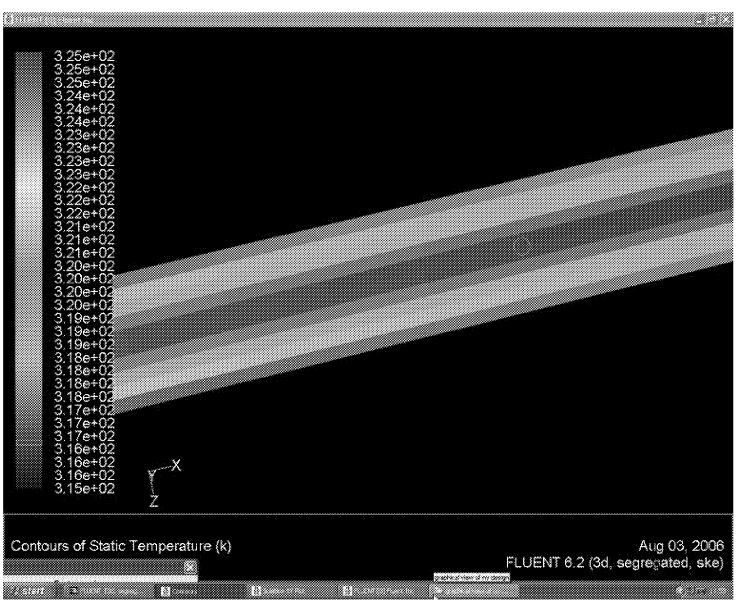

Figure 41: Representation of development of temperature in the fluid between the fins

Assessment of the thickness of the thermal and flow boundary layer ($\frac{\partial T}{\partial z}$ versus $\frac{\partial V}{\partial z}$) can be performed by comparing the figures (40) and (41). The middle layer in figure (40) represent the bulk air velocity that is 2m/sec the other layers at both sides of bulk velocity layer involve the flow boundary layer.
The middle zone temperature of the flow in figure (41) is about 317°C which differs from the inlet air flow temperature. Therefore there is no bulk temperature in figure (41). This is due to mixing of two thermal boundary layers at both sides of the middle flow. Figure (42) depicts the thickness of the thermal and flow boundary layers in the spacing of two typical fins of the heatsink.

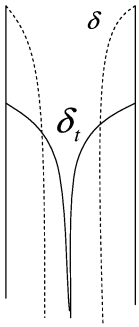

Figure 42: Development of thickness of thermal and velocity boundary layer
Pr <1 and $\delta_t > \delta$

Air temperature is lowest in the middle space between two fins. Maximum air temperature may be found near the plate surface or at the surface of the fin where the air velocity is zero. Thermal boundary layer is not uniform along the fins. Those parts of the fins that are located out of the base zone have particular thinner thermal boundary layer thickness than those parts that are settled in the base.

14. Conclusion

The impact of the fin configuration on thermal characteristic of the heatsink is investigated.
In addition to surface area and larger flow velocity, the fin profile is another solution in thermal management. A new manufacturing approach of copper heatsinks is proposed and the prototypes are examined experimentally and by numerical methods.
Airflow behavior and thermal characteristic of the proposed inclined free fin heatsink is studied by CFD codes.

A bigger fins-holder than source is proposed if the cross section area of the source is wider than the total cross section area of the bundled fins.

The significance of inclined free-fins heatsink is sensed when enhancement of heat fluxes or number of the transistors per unit area of electronic equipments is regarded. The limitation of this heat sink is the total area of the bundled foot part of the fins, which prohibits applying the same heat flux at larger areas. The total fin foot area is depended on thickness and number of the applied fins.

A 40 % scale up of the model is accomplished in the numerical framework. Applying the nonuniform cross sectional fins in heatsinks application by mechanical manufacturing approach may results in “about” the same performance as for scaled up heatsink in this study. Because the gaps are more spacious when using nonuniform cross sectional fins which improves the forced-convection heat transfer coefficient. Using the nonuniform copper fins in the heatsink application is suggested for higher heat fluxes and a mechanical construction method as described in this paper.

Modification of the fin foot height performs optimization in the CFD environment. The best result is achieved for 3mm height of fin foot.

An approach for mechanical manufacturing for another copper heatsink (flat plate) is introduced including design of the base and fins.

The thermal model used for the modeling the heatsink is a three- dimensional finite volume method. The computational domain in CF environment includes a heatsource maintained at the bottom of the base, heatsink and airflow through the heatsink. Flexibility of this design is of importance because using the thinner plates and base can diminish the effect of high density copper materials.

Flow behavior is studied at two different locations i.e. between the fins and in the passage in the middle of the heatsink.

The performance of the proposed model computed by the numerical calculation is high compared to current heatsinks as expected of the previous studies of double- part plates (foot and head).
Pressure drop, resulting from a configuration with high fin number, is acceptable until the optimized thermal performance is achieved.
Moderate pressure drop is observed through the fins of this heatsink that indicates proper fin spacing which does not result in mixing of two thermal boundary layers. This method serves as a proper indication of optimized number of the fins and fin spacing which give rise to a good management of thermal projects.

14.1 Future work

In order to enlarge the cross section area without increasing the number of fins, employing the non-uniform cross section type of straight fins is a practical solution.
Triangular and parabolic configuration of non-uniform cross-section fin is presented below.

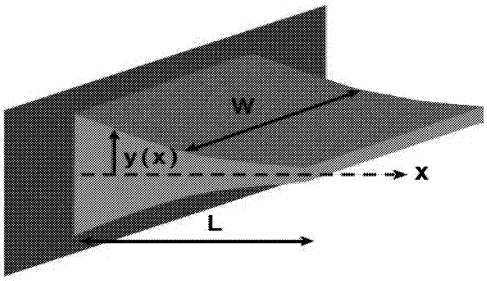

Figure43: Longitudinal fin of parabolic profile

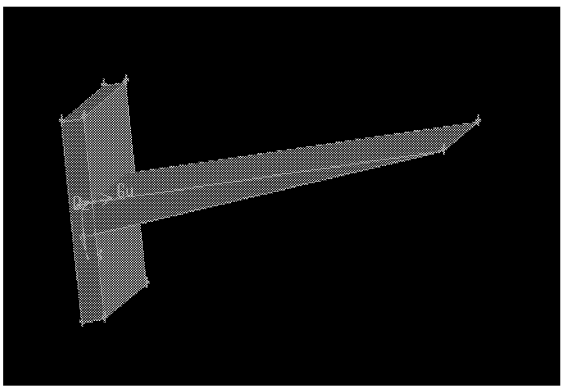

Figure44: Longitudinal fin of triangular profile

The other future work will be the employment of the inclined free fins upside down to eliminate any using of the base and limitations of the subsequent model as discussed in the former sections. Bundling the plates will accomplish either by using a ring around the fins or a head instead a foot part for the fins.

References

[1] Seri Lee, Arvid Thermal technologies, How to select a heat sink

[2] Robert E. Simons, Associate Editor, IBM Corporation, Simple Formulas for Estimating Thermal Spreading Resistance

[3] Jukka rantala ,associate editor , Nokia research centre, Surface flatness

[4] Ning Zheng and R. A. Wirtz, Mechanical Engineering Department, cylindrical pin fin fan-sink heat transfer and pressure drop correlations, University of Nevada, Reno

[5] Adam v barrett Izundu f obinelo Characterization of longitudinal fin heat sink thermal performance and flow bypass effects through CFD method

[6] C.K. Loh, D.J. Chou Comparative Analysis of Heat Sink Pressure Drop Using Different Methodologies

[7] Catharina R. Biber, Pressure drop and heat transfer in an isothermal channel with impingement flow, 1997, IEEE, page 224-230

[8] Robert E. Simons, Associate Editor, Estimating the Effect of Flow Bypass on Parallel Plate-Fin Heat Sink Performance, IBM Corporation

[9] Song, S., Lee, Sl, and Au, V., Thermal Spreading Resistance, 1994, "Closed-Form Equation for Thermal Constriction/Spreading Resistances with Variable Resistance Boundary Condition," Proceedings of the 1994 International Electronics Packaging

[10] Spreading Resistance of Isoflux Rectangles
and Strips on Compound Flux Channels, Microelectronics heat transfer laboratory, February 1998

[11] Spreading Resistance of Circular Sources on Compound and Isotropic Disks, microelectronics heat transfer laboratory, February, 1998 Conference, Atlanta, Geoergia, pp. 111-121.

[12] Barry Dagan ,Pin Fin Heatsinks Supply Compact Cooling Power, Sep1,2002 Cool Innovations Inc., Concord, Ontario, Canada

[13] Johnny S. Issa, Alfonso Ortega Experimental measurements of the flow and heat transfer of a square jet impinging on an array of square pin fins

[14] Adrian Bejan, Heat transfer, 1993, John Wiley & Sons page 219-245

[15] J. P Holman, Heat transfer, SI Metric Edition 1989,McGRAW-HILL book company, page 43-50, 220-245

[16] Frank P. Incropera, David p. Dewitt, Fundamental of heat and mass transfer, fourth edition 1996, John Wiley & Sons page 284-300

[17] Fluent 6 user's guide publications 2001 volume 1 chapter 6 page 3-90

[18] Fluent 6 user's guide publications 2001 volume 2 chapter 11 page2-20

[19] Sridhar Narasimhan, Avaram Bar-Cohn, Rjish Nair , Thermal compact modeling of parallel plate heatsinks 2003,IEEE, vol.26,nr.1 -page 136-146

[20] Frank Kreith, Principles of heat transfer, third edition 1976Harper & Row publishers page 309-318

[21] Massoud Kaviani, Principles of heat transfer,2002,John Wiley & Sons, page 40-80, 120-123

[22] R. Byron Bird, Warren E Stewart, Edwin N. Lightfoot, Transport phenomena second edition, John Wiley & Sons 2002,

[23] M. Necati özisik, Finite difference methods in heat transfer, CRC press Inc. Page 20-40

[14] Victor L. Streeter , E. Benjamin, Wylie fluid mechanics 1983, McGraw-Hill book company page 88-100 , 195-198

[24] Brucer R. Munson, Donald F. Young, Theodor H. Okishi, Fundamentals of fluid mechanics third edition,1998, John Wiley & Sons pages

[25] J. P. Holman, Heat transfer, SI metric edition, 1989, McGraw-Hill book company

[26] Frank Kreith, Principles of heat transfer, third edition 1976 Harper & Row, publishers

[27] Lee, S., Song, S., Au, V., and Moran, K.P., "Constriction/spreading resistance Model for Electronic Packaging," Proceedings of ASME/JSME Engineering Conference, Vol. 4, 1995.